

Climatology of quasi-2-day wave structure and variability at middle latitudes in the northern and southern hemispheres



Hiroyuki Iimura ^{a,*}, David C. Fritts ^a, Ruth S. Lieberman ^b, Diego Janches ^b, Nicholas J. Mitchell ^c, Steven J. Franke ^d, Werner Singer ^e, Wayne K. Hocking ^f, Michael J. Taylor ^g, Tracy Moffat-Griffin ^h

^a GATS Inc., Boulder, CO, USA

^b NASA Goddard Space Flight Center, Greenbelt, MD, USA

^c Department of Electronic and Electrical Engineering, University of Bath, Bath, UK

^d Department of Electrical and Computer Engineering, University of Illinois Urbana-Champaign, IL, USA

^e Leibniz Institute of Atmospheric Physics, Rostock University, Kühlungsborn, Germany

^f Department of Physics, University of Western Ontario, London, Ontario, Canada

^g Space Dynamics Laboratory and Physics Department, Utah State University, UT, USA

^h British Antarctic Survey, Cambridge, UK

ARTICLE INFO

Keywords:

Mesosphere and lower thermosphere

Quasi-2-day wave

Planetary wave

Aura satellite

ABSTRACT

Climatological structure of the quasi-2-day wave (Q2DW) at middle latitudes in temperature and horizontal winds in the mesosphere and lower thermosphere (MLT) was compared between the northern and southern hemispheres. Determination of the Q2DW in temperature was based on observation data by the Microwave Limb Sounder (MLS) onboard NASA's Earth Observing System (EOS) Aura satellite over 17 years from August 2004 to May 2021 and the Q2DW in horizontal winds was derived from Aura/MLS geopotential height data using balance equations. Amplitudes were maximized in summer in the southern hemisphere and in the meridional wind in the northern hemisphere, but in winter in the zonal wind in the northern hemisphere. Summer amplitudes were larger in the meridional wind than the zonal wind in the southern hemisphere, but zonal amplitudes in winter were larger than meridional amplitudes in summer in the northern hemisphere. Westward propagating zonal wavenumber 3 (W3) was largest in both hemispheres, but in addition to well-known W4, W3, W2 and eastward propagating zonal wavenumber 2 (E2), we also found W1, zonally symmetric standing (SO), and E1. Eliassen-Palm fluxes were derived for each mode. W3, W2, W1, and E2 fluxes were exhibited upward and poleward in January in the southern hemisphere while only W3 fluxes were exhibited clearly upward and poleward in July in the northern hemisphere. The balance winds and radar winds agreed in both amplitude and phase in the southern hemisphere and at lower latitudes in the northern hemisphere in January, and at lower latitudes in both hemispheres in July. Furthermore, the Q2DW is modulation in amplitude and phase from the W3 by accumulating other modes.

1. Introduction

The quasi-2-day wave (Q2DW) is a global phenomenon and, since its discovery, has been observed in atmosphere from earth's surface through the troposphere to the thermosphere. In particular, the Q2DW in the mesosphere and lower thermosphere (MLT) has been observed by ground-based and satellite measurements (Bristow et al., 1999; Fritts et al., 1999; Kulikov, 2007; Li et al., 2008; Morris et al., 2009; Riggan et al., 2004; Sandford et al., 2008).

Salby (1980, 1981a, 1981b) proposed that the Q2DW is a manifestation of the mixed Rossby-gravity (3, 0) normal mode with a period of ~ 2.25 days and Pfister (1985) inferred wave growth of zonal wavenumbers 2, 3, and 4 with periods of ~ 2 days. Hagan et al. (1993) showed that the (3, 0) mode is sensitive to zonal mean winds, especially a combination of weak eastward winds in the northern hemisphere and westward winds in the southern hemisphere in the MLT. Plumb (1983) theoretically predicted a growth of the Q2DW by baroclinic instabilities caused by an eastward shear in a westward jet, and this was investigated

* Corresponding author.

E-mail address: iimura@gats-inc.com (H. Iimura).

employing satellite observations (Gu et al., 2013; Lieberman, 1999; Limpasuvan and Dong, 2009).

Relations between the Q2DW and baroclinic/barotropic instabilities have also been examined employing model simulations (Baumgaertner et al., 2008; Guharay et al., 2013; McCormack et al., 2009; Merzlyakov and Jacobi, 2004; Rojas and Norton, 2007; Salby and Callaghan, 2001, 2003; Schröder and Schmitz, 2004; Yue et al., 2012b) although Hunt (1981) showed only minimal baroclinic activity. Furthermore, Jia et al. (2012) and Offermann et al. (2011) inferred that Q2DW amplitudes correspond to the meridional gradient of the quasi-geostrophic potential vorticity; and Salby (1981c) concluded that Q2DW amplitudes grow with altitude where refractive index increases and temperature decreases equatorward. Pendlebury (2012) suggested a significant source of Q2DW variability for polar mesospheric clouds, Gurubaran et al. (2001a) found a correlation with the equatorial electrojet, and Sonnemann and Grygalashvily (2005) found a 2-day oscillation in a photochemical system in the MLT.

Q2DW analyses employing ground-based radar wind measurements at various locations have shown that Q2DW responses are enhanced in summer and winter with meridional amplitudes larger than zonal amplitudes. Although the response is maximized in late January in the southern hemisphere (Hecht et al., 2010; Lima et al., 2012; Murphy and Vincent, 1998; Poole, 1990; Poole and Harris, 1995; Takahashi et al., 2012), amplitudes in the northern hemisphere are larger primarily in summer (Chshyolkova et al., 2005; Jacobi et al., 1997, 1998; Malinga and Ruohoniemi, 2007; Namboothiri et al., 2002; Thayaparan et al., 1997a, 1997b), but can also be larger in winter (Gurubaran et al., 2001b; Nozawa et al., 2003a). A vertical wavelength is variable at 25–100 km at low and equatorial latitudes (Araújo et al., 2014; Gurubaran et al., 2001b; Harris et al., 2013; Lima et al., 2004) but can be > 150 km at middle latitudes (Craig and Elford, 1981; Harris, 1994; Tsuda et al., 1988).

Interhemispheric comparisons of simultaneous radar wind measurements at middle latitudes (Craig et al., 1983; Tsuda et al., 1988) and high latitudes (Tunbridge and Mitchell, 2009) revealed that Q2DW amplitudes in summer were larger in the southern hemisphere than northern hemisphere for both zonal and meridional components.

By combining radar wind measurements at multiple locations, discrepancies from westward-propagating zonal wavenumber 3 (W3) structure were found in January in both southern (Craig et al., 1980) and northern (Nozawa et al., 2003b) hemispheres. At middle latitudes in the northern hemisphere, Meek et al. (1996) found W3 as well as westward propagating zonal wavenumber 4 (W4), Merzlyakov et al. (2004) found westward propagating zonal wavenumber 2 (W2), W3, and W4 in 80, 60, and 48 h, respectively, and Pancheva et al. (2004) found W2, W3, and W4 in 53–56, 48–50, and 42–43 h, respectively. At low latitudes in the northern hemisphere, Pancheva et al. (2006) and Kumar et al. (2018) found W2 in the Q2DW.

The spatial structure of Q2DW zonal wavenumbers has been studied employing satellite measurements of winds (Ward et al., 1996; Wu et al., 1993), temperature (Huang et al., 2013; Rodgers and Prata, 1981; Tunbridge et al., 2011; Wu et al., 1996), OH airglow (Pedatella and Forbes, 2012), water vapor (Limpasuvan and Leovy, 1995; Limpasuvan and Wu, 2003), and ozone density (Azeem et al., 2001). These satellites include Nimbus 5 Selective Chopper Radiometer (SCR), Nimbus 6 Pressure Modulated Radiometer (PMR), Microwave Limb Sounder (MLS) onboard the Upper Atmosphere Research Satellite (UARS) and the Earth Observing System (EOS) Aura satellite, the High Resolution Doppler Imager (HRDI) and the Wind Imaging Interferometer (WINDII) onboard UARS, and the Sounding of the Atmosphere using Broadband Emission Radiometry (SABER) onboard the Thermosphere Ionosphere Mesosphere Energetics Dynamics (TIMED) satellite. Their results showed that.

1. Q2DW amplitudes in summer enhancements were much larger in the southern hemisphere than the northern hemisphere,

2. W3 was dominant during summer enhancements in the southern hemisphere, maximizing at $\sim 30^{\circ}$ S while a mixture of W3, W4, and W2 in the northern hemisphere, and
3. The Q2DW was anti-symmetric with respect to the equator.

Recent studies of global Q2DW structure employing satellite measurements have been focused mainly on temperature, while spatial structure of the Q2DW in wind fields differs from temperature with significant interannual variabilities. The Q2DW in zonal and meridional winds has been studied from ground-based radar observations. However, it is impossible to determine latitudinal variabilities of the Q2DW for each zonal wavenumber from ground-based observations at sparse locations. Study of Q2DW modes has mostly been focused on W3 in the southern hemisphere and additionally W4 and W2 in the northern hemisphere. Therefore, we studies other zonal wavenumber modes, such as W1, S0, and eastward propagations. Recently, Fritts et al. (2019) examined the spatial structure of the Q2DW in horizontal winds in January 2015 in the southern hemisphere, derived from balance equations with MLS geopotential height data. The wind data reasonably agreed with the Q2DW radar wind measurements. They also showed Eliassen-Palm (EP) fluxes for each Q2DW zonal wavenumber. We will apply their analyses to compare spatial structure of the climatological Q2DW in the southern and northern hemispheres in January and July. Because we slightly modified their methodology to estimate Q2DW winds inferred from MLS/balance equations to avoid aliasing between the Q2DW and longer-period planetary waves and to minimize uncertainties of the Q2DW, our methodology is explained in the next section. Results are presented in Section 3. Discussion and summary are described in Sections 4 and 5.

2. Data acquisition and analysis methodology

2.1. Aura/MLS

NASA's EOS Aura satellite launched on July 25, 2004 into a near-polar sun-synchronous orbit at an altitude of 705 km and orbits ~ 15 times per day. The MLS onboard Aura began observing thermal microwave emission from Earth on August 14, 2004 at 55 pressure levels between 1000 and 10^{-5} hPa. The MLS measures global atmospheric temperature and constituents day and night. Geopotential height is computed from integration of the hydrostatic equation (Schwartz et al., 2008).

We basically followed the analysis methodology of Fritts et al. (2019) for Q2DW zonal and meridional winds from MLS data. However, their methodology is valid only when the Q2DW dominates atmospheric waves, e.g., in January in the southern hemisphere. To analyze seasonal variabilities of the Q2DW in both northern and southern hemispheres extracted from longer-period planetary waves, we modified their methodology slightly.

Aura/MLS temperature and geopotential height data were collected in bins of 24° in longitude, 5° in latitude, and 12-h universal time (UT) for each altitude between 70 and 97 km. Then, 10-day zonal mean temperature and geopotential height were computed. If the data were collected continuously, all bins were filled by the data. However, data were sometimes missing. These bins were interpolated by a cubic spline with three degrees of freedom, and a band-pass filter between 42 and 54 h was applied to time series for each longitude, latitude, and altitude. The band-pass filtered data enabled 10-day least-square fits to sinusoids with westward propagating zonal wavenumbers 1, 2, 3, and 4 (W1, W2, W3, and W4), zonally symmetric mode (S0), and eastward propagating zonal wavenumbers 1 and 2 (E1 and E2) for a 48-h period. Although a period range between 42 and 54 h is relatively narrow for the Q2DW, we decided to use it to obtain 10-day mean Q2DW amplitudes with smaller uncertainties at the fits. Because periods of the Q2DW were reported longer for the W4 and shorter for the W2 than 48 h, our results of W4 and W2 amplitudes may be smaller than actual values. The methodology

previously used by Fritts et al. (2019) had a small alias between the Q2DW and longer-period planetary waves with the same zonal wavenumber, therefore, the alias was solved by employing the band-pass filter before computing the least-square fits.

Amplitudes and phases in zonal and meridional winds for each zonal wavenumber were estimated from geopotential height Q2DW amplitudes and phases employing zonal and meridional momentum equations (Hitchman et al., 1987),

$$\partial u'/\partial t + \bar{u} (\partial u'/\partial \lambda) / (a \cos \varphi) - f_1 v' = - (\partial \Phi' / \partial \lambda) / (a \cos \varphi), \quad (1)$$

and

$$\partial v'/\partial t + \bar{u} (\partial v'/\partial \lambda) / (a \cos \varphi) - f_2 u' = - (\partial \Phi' / \partial \varphi) / a, \quad (2)$$

where u' , v' , and Φ' are perturbations of zonal and meridional winds, and geopotential height, φ and λ are latitude and longitude, a is Earth's radius, and \bar{u} is a zonal mean zonal wind, which was estimated from zonal mean geopotential heights, assuming gradient wind balance (Hitchman and Leovy, 1986; Hitchman et al., 1987),

$$\bar{u} = - (1/f) (\partial \Phi' / \partial y) [1 - (1/f) (\partial \Phi' / \partial y) / (2\Omega a \cos \varphi)]^{-1}, \quad (3)$$

where $\Omega = 2\pi$ (day⁻¹) and $f = 2\Omega \sin \varphi$. f_1 and f_2 are defined as

$$f_1 = 2\Omega \sin \varphi - [\partial(\bar{u} \cos \varphi) / \partial \varphi] / (a \cos \varphi), \quad (4)$$

and

$$f_2 = 2\Omega \sin \varphi + 2\bar{u} \tan \varphi / a. \quad (5)$$

The Q2DW results presented in the next section are the accumulation of all zonal wavenumbers.

The meridional and altitudinal components of EP flux (Andrews et al., 1987) were computed by

$$F^\Phi = (\partial \bar{u} / \partial z) \langle v' \theta' \rangle / (\partial \theta_0 / \partial z) - \langle u' v' \rangle, \quad (6)$$

and

$$F^w = [f - (a \cos \varphi)^{-1} \partial(\bar{u} \cos \varphi) / \partial \varphi] \langle v' \theta' \rangle / (\partial \theta_0 / \partial z) - \langle u' w' \rangle, \quad (7)$$

where θ is geopotential temperature and $\langle \rangle$ indicates a zonal mean. EP fluxes presented in the next section were normalized by $\rho_0 a \cos \varphi$ for both components.

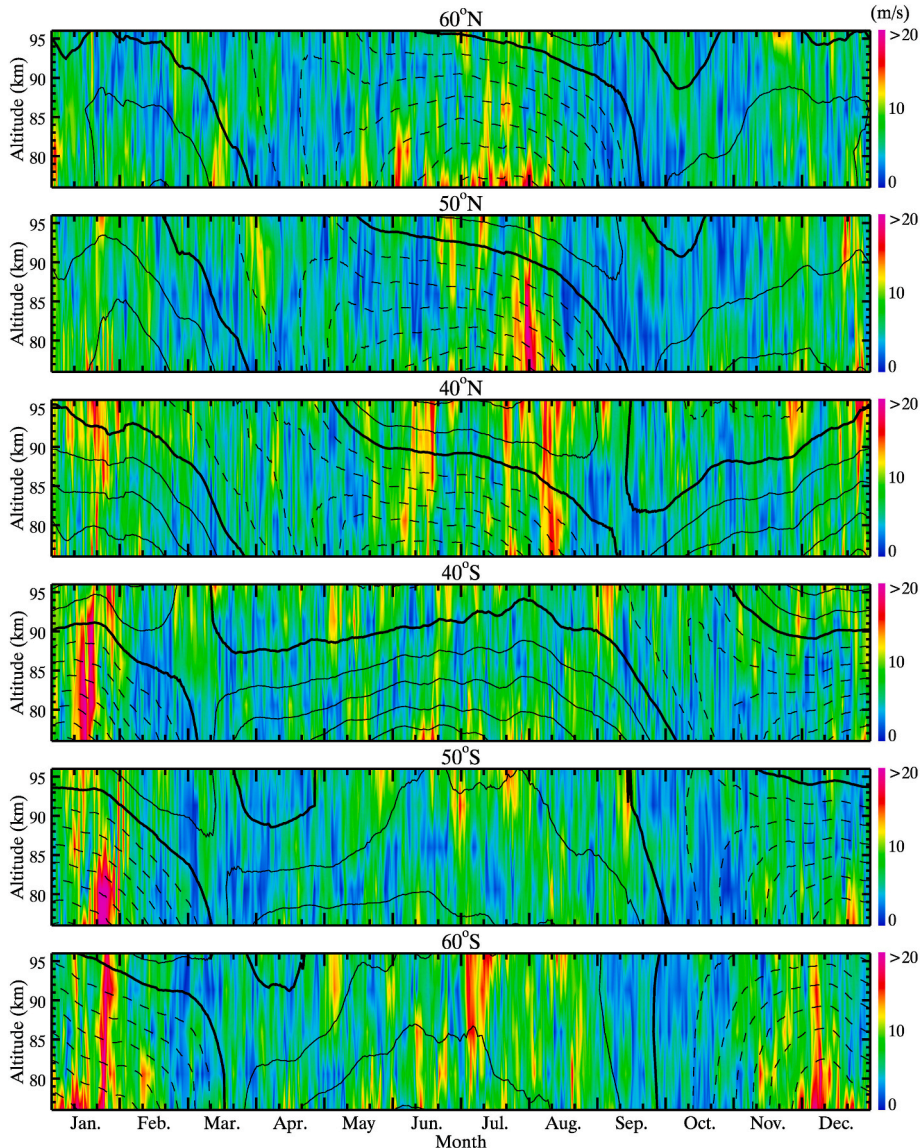


Fig. 1. Q2DW amplitudes at 0° in longitude of the zonal component induced by MLS/balance winds as a function of altitude at 60°N, 50°N, 40°N, 40°S, 50°S, and 60°S from top to bottom. Line contours indicate zonal mean zonal winds every 10 m/s. Thick lines indicate 0 m/s and solid and dashed lines are eastward and westward.

2.2. Meteor radars

Six meteor radars were employed at roughly conjugate latitudes in each hemisphere to compare with MLS/balance winds. All of these are All-Sky Interferometric Meteor Radar (SkiYMet) located at Esrange (68°N , 21°E), Juliusruh (55°N , 14°E), Bear Lake Observatory (42°N , 111°W), Cerro Pachón (30°S , 71°W), Tierra del Fuego (54°S , 68°W), and Rothera Station (68°S , 68°W) to minimize systematic biases and determine hourly winds under the same conditions. Determinations of hourly winds are described by Iimura et al. (2015). Meteor echo data at 90 ± 1.5 km were collected, which had zenith angles between 10° and 70° , and hourly mean zonal and meridional winds were computed if there were at least five echoes. Missing hourly points were interpolated by a cubic spline with three degrees of freedom and time series of the Q2DW were determined by inversed fast Fourier transform with a band-pass filter at 42 and 56 h. Amplitudes and phases of the 10-day mean Q2DW were estimated by least-square fits to sinusoids with 48 h.

3. Results

3.1. Spatial structure

Figs. 1 and 2 show seasonal and altitude variabilities of zonal and meridional Q2DW amplitudes at 0° longitude at six latitudes in an altitude range between ~ 85 and 95 km. Amplitudes maximized from July to August for both components at 50°N and 60°N and larger in the zonal component (>20 m/s) decreasing with altitude compared to the meridional component (<20 m/s) which increased with altitude. At 40°N , amplitudes maximized at ~ 21 m/s at 97 km in January for the zonal component and from July to August for the meridional component which increased with altitude, maximizing at ~ 22 m/s at 97 km. In the southern hemisphere, maximum amplitudes were in January at all latitudes for both components, ranging from 23 to 32 m/s, but amplitudes were also enhanced from June to July at all latitudes for the zonal component (<8 m/s) and at 60°S for the meridional component (~ 6 m/s). Although amplitudes increased with altitude in late January at 60°S for the zonal component and at all latitudes for the meridional component, amplitudes decreased with altitude at 40°S and 50°S for the zonal component and increased with altitude from June to July at all latitudes

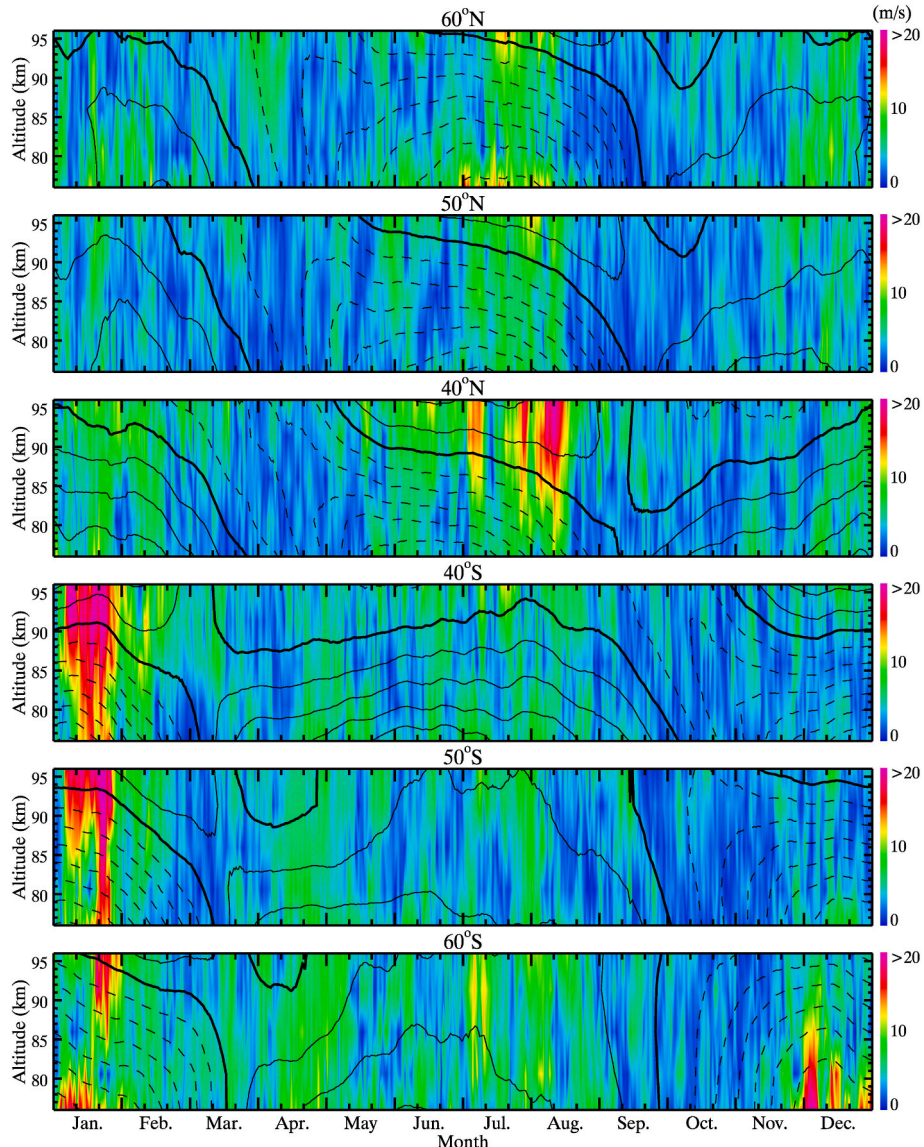


Fig. 2. Same as Fig. 1, but for meridional component.

for both components. Responses were also strong at 60° S from December to early January for both components, weakening with altitude.

The upper panels of Fig. 3 show seasonal and latitudinal variabilities of Q2DW amplitudes at 0° longitude at 91 km. For the zonal component, amplitudes maximized in January at 35° in both hemispheres (28 m/s in the northern hemisphere and 24 m/s in the southern hemisphere), and additionally at 60° S in late January. Zonal amplitudes did not have a clear trend with latitude in both hemispheres. For the meridional component, the Q2DW was clearly a summer phenomenon in both hemispheres, increasing in amplitude equatorward and maximizing at >22 m/s in both hemispheres. Amplitudes were moderately enhanced in winter in both hemispheres, but increased equatorward in the northern hemisphere and maximized at 60° S in the southern hemisphere.

The lower panels of Fig. 3 compare latitudinal structures of Q2DW amplitudes at 0° longitude in the northern and southern hemispheres in January and July at 91 km. As shown in the upper panels of Fig. 3, amplitudes were larger in January than July for the zonal component in both hemispheres. Zonal amplitudes maximized at <28 m/s at $<45^{\circ}$ N from 18 January in the northern hemisphere while amplitudes maximized at <27 m/s at $\sim 45^{\circ}$ S until 20 January and then, at $\sim 40^{\circ}$ S and 60° S in the southern hemisphere. For the meridional component in the

southern hemisphere, amplitudes maximized at <24 m/s from 5 to 18 January between 40° S and 50° S, between 20 and 23 January at all latitudes, and then at $\sim 50^{\circ}$ S. In the northern hemisphere, maxima of meridional amplitudes were at $<35^{\circ}$ N in January and at $<45^{\circ}$ N before 10 July and after 20 July.

Fig. 4 shows latitudinal variabilities of Q2DW amplitudes for each zonal wavenumber at 91 km in January and February. Maximum amplitudes were larger for all modes and both components in the southern hemisphere than the northern hemisphere, but maxima in the northern hemisphere were nearly equivalent to maxima in the southern hemisphere for W2, W1, S0, and E1 in the zonal component. Additionally, zonal maxima for these W2, W1, S0, and E1 were larger than meridional maxima in both hemispheres. W4 amplitudes increased equatorward for both components in the southern hemisphere and maximized from late January to early February. W3 amplitudes maximized on ~ 20 January for both components in the southern hemisphere, but at $\sim 47^{\circ}$ S in the zonal component and increased equatorward in the meridional component. W3 amplitudes in the northern hemisphere maximized later than the southern hemisphere and increased equatorward for both components. E2 amplitudes maximized equatorward of 40° S in late January and at $\sim 55^{\circ}$ S moderately for both components.

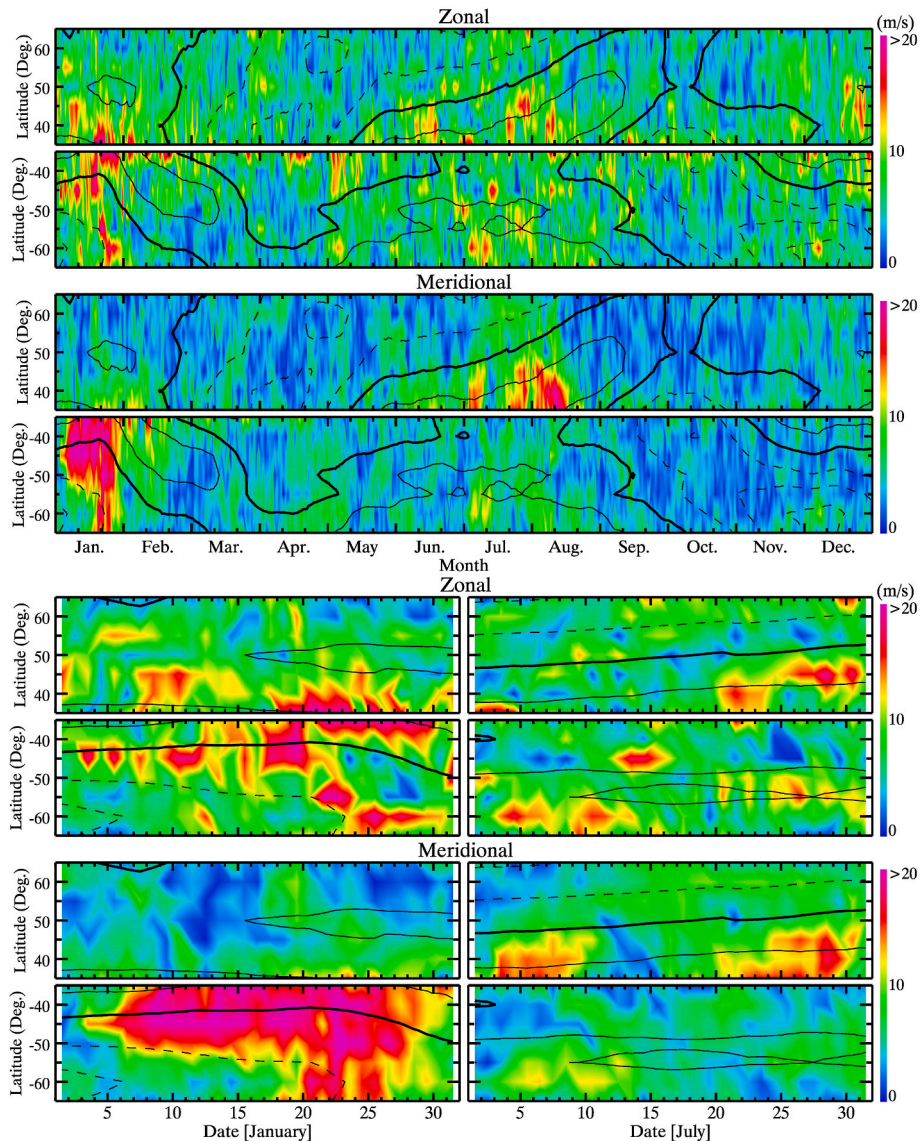


Fig. 3. (Top) Q2DW amplitudes at 0° in longitude induced by MLS/balance winds at 91 km as a function of latitude. (Bottom) Q2DW amplitudes of the (upper) zonal and (lower) meridional components for (left) January and (right) July. Line contours are same as defined in Fig. 1.

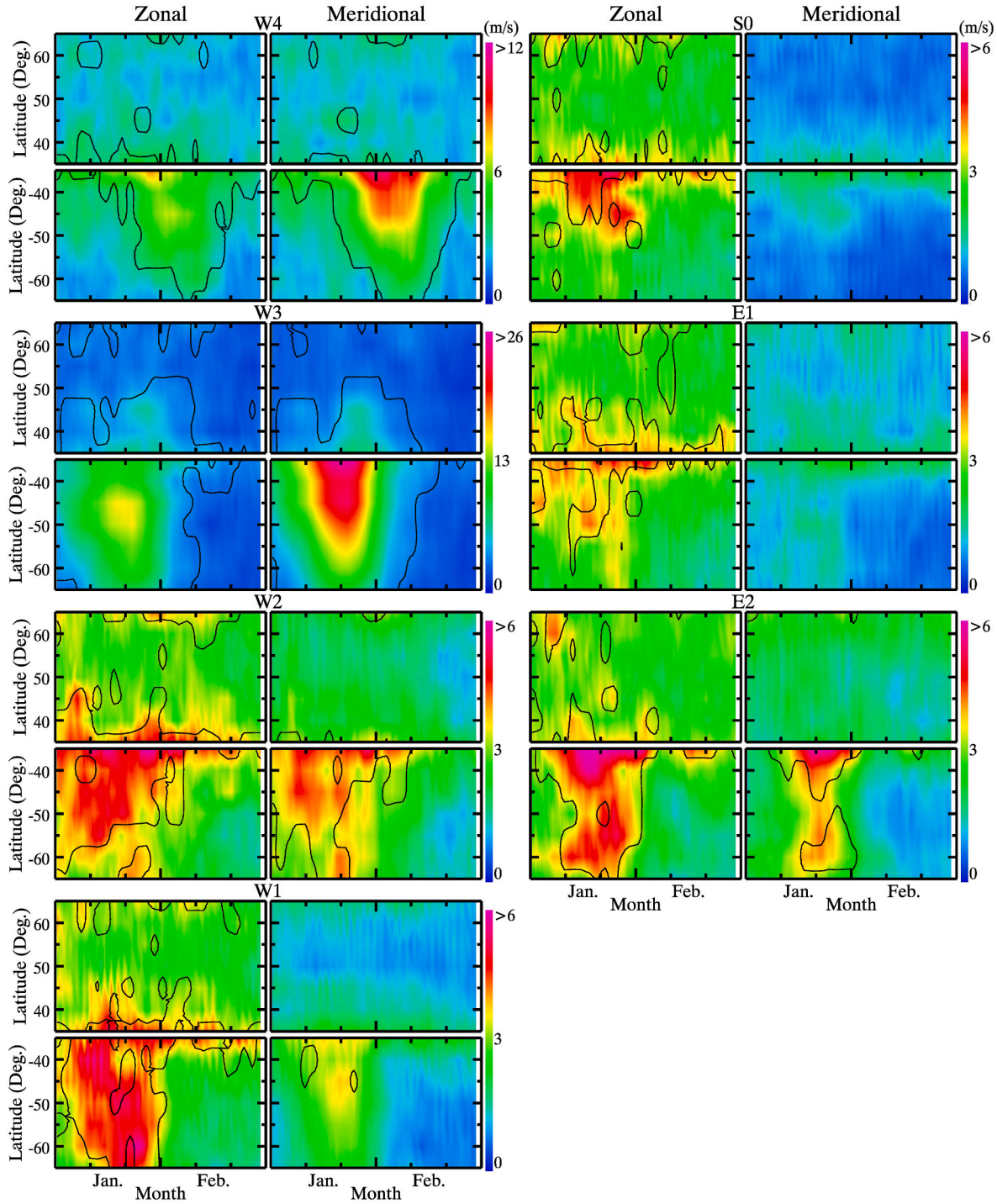


Fig. 4. Q2DW zonal and meridional wind amplitudes induced by MLS/balance winds at 91 km as functions of latitude in January and February. (Left) W4 to W1 and (right) S0 to E2 are shown from top to bottom. Results of 95% significance level test are shown in line contours.

Similarly, Fig. 5 shows latitudinal variabilities of Q2DW amplitudes for each zonal wavenumber at 91 km in July and August. Like amplitudes in January in the southern hemisphere, zonal maxima for W2, W1, S0, and E1 were larger than meridional maxima in both hemispheres increasing equatorward for both components. W4 amplitudes increased equatorward in the northern hemisphere and maximized in early August for both components. Latitudinal structure of W3 was similar to W4 in the northern hemisphere for both components but W3 amplitudes maximized earlier than W4 at ~ 8 m/s for the zonal component and >12 m/s for the meridional component. E2 amplitudes increased equatorward for the zonal component in the northern hemisphere, but

maximized at $>60^\circ$ S in the southern hemisphere in early July for both components and early August only for the zonal component.

Fig. 6 shows latitude/longitude structures of the Q2DW in winds and temperature for each zonal wavenumber at 91 km at 12:00 on 22 January. Amplitudes were larger in the southern hemisphere than the northern hemisphere for both winds and temperature. Temperature amplitudes maximized at $<50^\circ$ S for all modes. In the zonal wind, W3 and W2 amplitudes maximized at ~ 15 m/s and 5 m/s at $\sim 40^\circ$ S and W1 maximized at ~ 5 m/s at 55° S. In the meridional wind, amplitudes maximized at $<35^\circ$ S for all modes except W1, which maximized at ~ 4 m/s at 45° S. Phase structures with respect to the equator were:

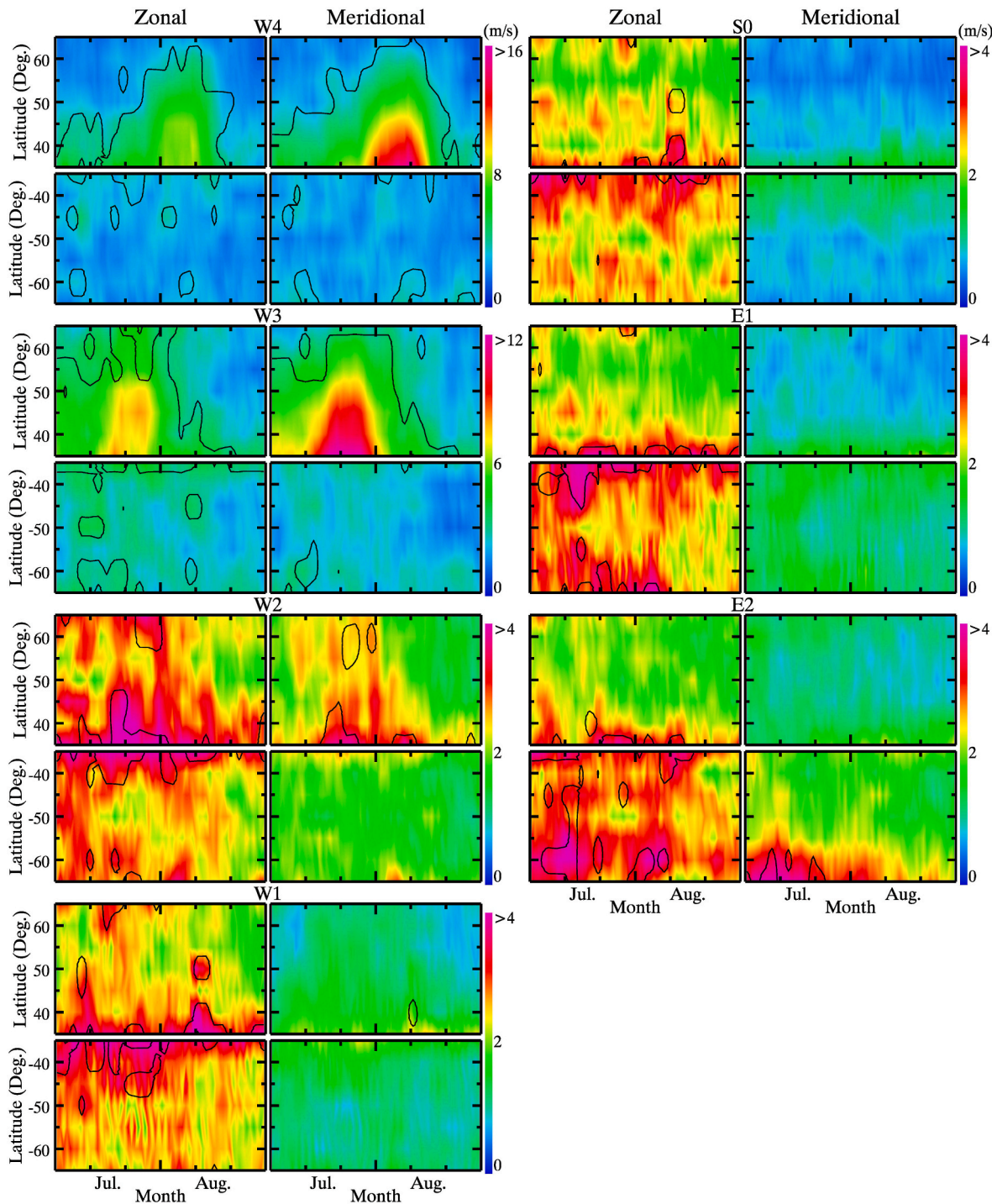


Fig. 5. Same as Fig. 4, but for July and August.

W4: anti-symmetric (symmetric) at $<50^\circ$ in temperature (zonal wind).

W3: anti-symmetric (symmetric) at $<40^\circ$ in temperature and zonal (meridional) wind.

W2: anti-symmetric (symmetric) in temperature and meridional (zonal) wind.

W1: anti-symmetric at $>50^\circ$ in temperature.

S0: anti-symmetric (symmetric) in zonal (meridional) wind.

E1: anti-symmetric in temperature and meridional wind, and.

E2: anti-symmetric at $<40^\circ$ in all components.

Temperature and meridional winds were mostly anti-phase for all

modes, except for E1 in the southern hemisphere, but mostly inphase in the northern hemisphere. Zonal and meridional winds were nearly quadrature for all modes except for W2 in the southern hemisphere.

Similarly, Fig. 7 shows horizontal structures of winds and temperature on 28 July. Amplitudes maximized in the northern hemisphere for all modes, except for E1. Due to smaller amplitudes in July compared to January, phases were determined less confidently. However, some apparent features with respect to the equator were:

W4: symmetric at $<45^\circ$ in temperature and zonal wind.

W3: anti-symmetric (symmetric) in temperature and zonal (meridional) wind.

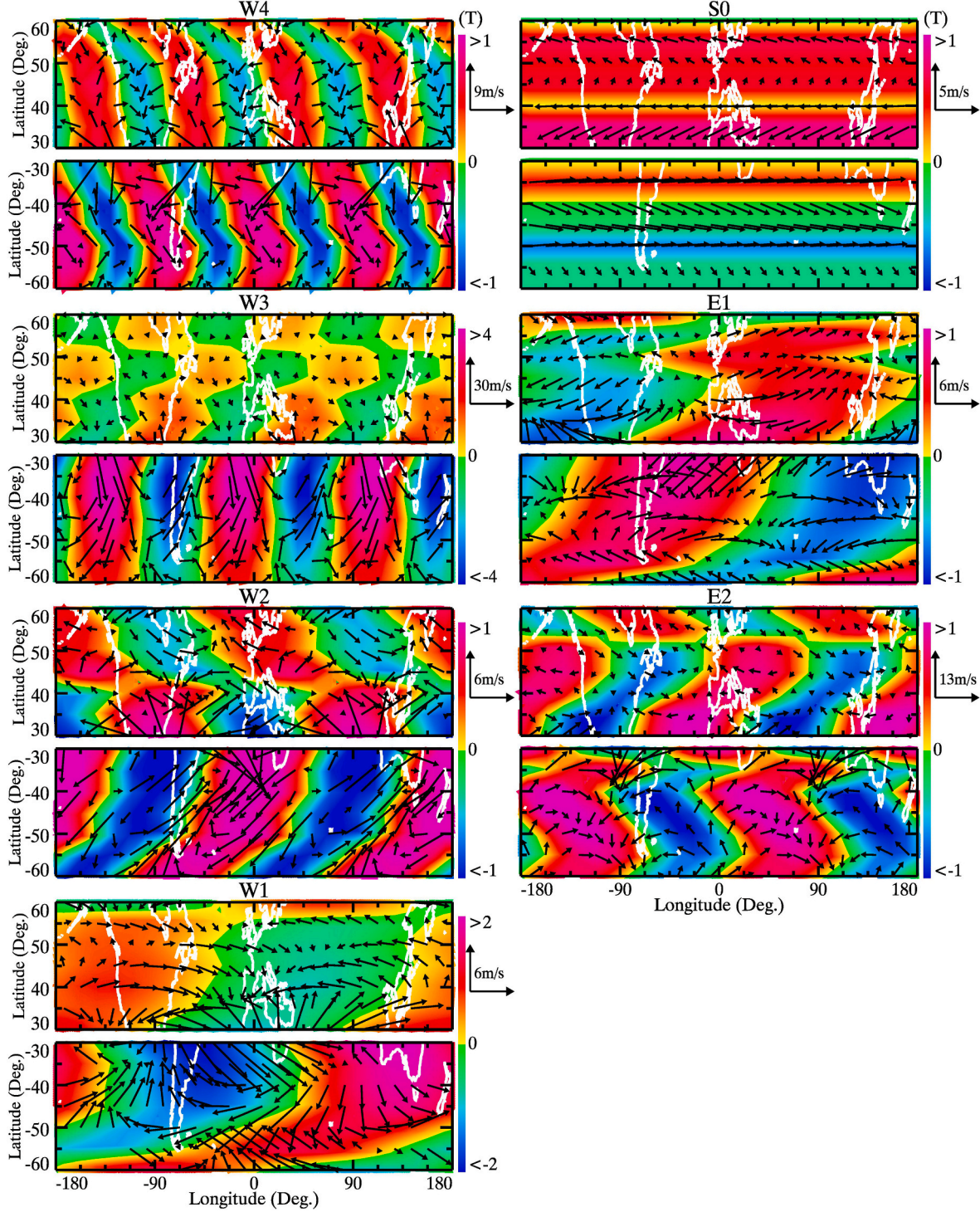


Fig. 6. Longitude/latitude variations of Q2DW horizontal balance winds and MLS temperature at 91 km at 12:00 on 22 January (left) from W4 to W1 and (right) from S0 to E2, and (right bottom) sum of all modes.

W2 and W1: symmetric in temperature and meridional wind.
 S0: anti-symmetric (symmetric) at $<40^\circ$ in temperature and meridional (zonal) wind.

E1: anti-symmetric (symmetric) at $<45^\circ$ in temperature (meridional wind) and reverse at $>45^\circ$, and.

E2: anti-symmetric (symmetric) in temperature (meridional wind).

In the northern hemisphere, temperature and meridional wind were mostly inphase for all modes, except for E2. W3 shows a Rossby-gravity normal mode in both January and July.

3.2. EP flux

Fig. 8 shows latitude/altitude cross sections of EP fluxes and divergence for each mode on 22 January. W3, W2, and W1 exhibit mostly poleward and upward fluxes at >80 km and $>40^\circ\text{S}$ in the southern hemisphere. However, divergence maximized at 40°S and 90 km for W3, and $<35^\circ\text{S}$ and >80 km for W2 and W1. E2 fluxes were mostly poleward but vertical fluxes were not clear. Maxima of E2 divergences were at $>50^\circ\text{S}$ and larger in magnitude than W2 and W1.

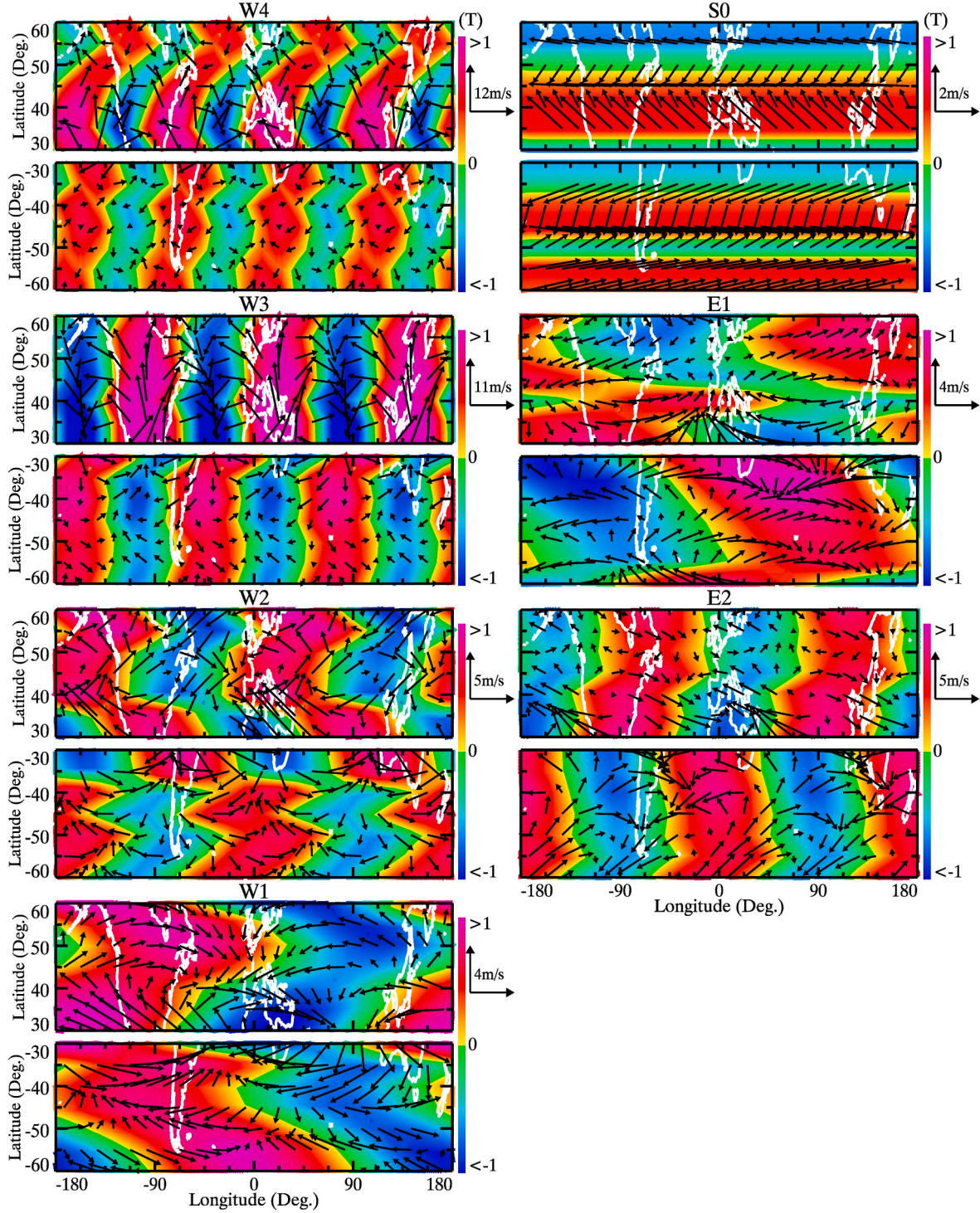


Fig. 7. Same as Fig. 6, but at 12:00 on 28 July.

Similarly, Fig. 9 shows latitude/altitude cross sections on 28 July. Fluxes were poleward and upward at >75 km for W3 and $<40^\circ\text{N}$ for W1 in the northern hemisphere. Divergences for W3 maximized at $<40^\circ$ in both hemispheres and minimized at ~ 80 km and 50°N . Fluxes for W2, W1, and E1 at <70 km were mostly upward and equatorward in the southern hemisphere with larger magnitudes than the northern hemisphere, and hence divergences for W2 and W1 maximized at <60 km and $\sim 60^\circ\text{S}$.

3.3. Comparison of balance and radar winds

Fig. 10 compares Q2DW meteor radar winds at six sites and balance winds at the closest latitudes in January 2012. As a reference, W3 balance winds are also shown. Although W3 dominated the Q2DW in the southern hemisphere, W3 amplitudes were smaller than radar amplitudes in the southern hemisphere. But Q2DW amplitudes of balance winds were larger than W3 amplitudes and comparable to radar amplitudes, especially for the meridional component at Cerro Pachón, zonal component at Tierra de Fuego, and both components at Rothera.

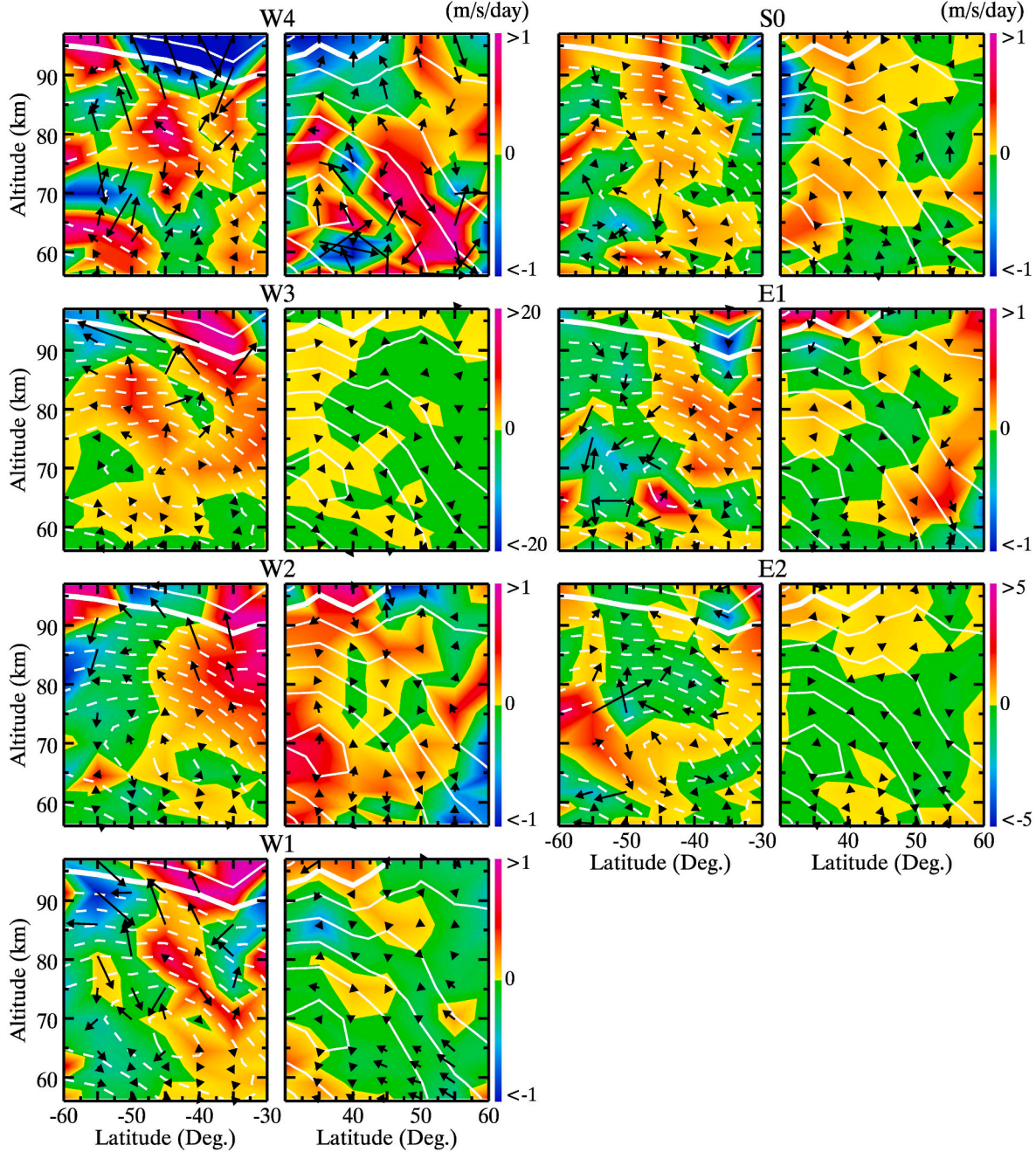


Fig. 8. Latitude/altitude cross section of EP fluxes for each zonal wavenumber mode (W4 to W1 on left and S0 to E2 on right) on 22 January. Color contours show EP flux divergence. White line contours indicate zonal mean zonal winds every 10 m/s with thick lines for 0 m/s and dashed lines for westward.

Therefore, all modes of the Q2DW had significant influence on the Q2DW in wind fields.

Although radar data are available until 18 January at Bear Lake and until 15 January at Cerro Pachón, The Q2DW agreed between radar winds and balance winds for the meridional component at Bear Lake and both components at Cerro Pachón. However, phases of the balance wind Q2DW were largely modulated from W3 by other modes at Bear Lake while phases of the W3 and balance wind Q2DW agreed at Cerro Pachón. Phases of the W3 and balance wind Q2DW were similar at Tierra del Fuego and Rothera and they agreed with radar wind phases while amplitudes of balance winds were slightly smaller than radar amplitudes at Tierra del Fuego for both components but larger or equivalent at Rothera. These results agreed with Fritts et al. (2019). At Juliusruh, Q2DW amplitudes of balance winds were larger than W3

amplitudes and the Q2DW agreed between balance winds and radar winds for both components after 18 January.

Similarly, Fig. 11 compares radar and balance wind Q2DW in July. The time series between these agreed best at Bear Lake. A W3 dominated the Q2DW and they agreed with the radar winds in both amplitude and phase before 22 July (between 21 July and 28 July) for the zonal (meridional) component. Amplitudes were larger in balance winds than radar winds after 24 July for the zonal component and in radar winds than balance winds before 23 July and after 27 July for the meridional component. Results at Juliusruh in July were similar to the results at Tierra del Fuego and Rothera in January (Fig. 10). The W3 dominated the Q2DW at Juliusruh and these amplitudes were slightly smaller than radar amplitudes. However, phases agreed between balance winds and radar winds. At Esrange, Tierra del Fuego, and Rothera, balance winds

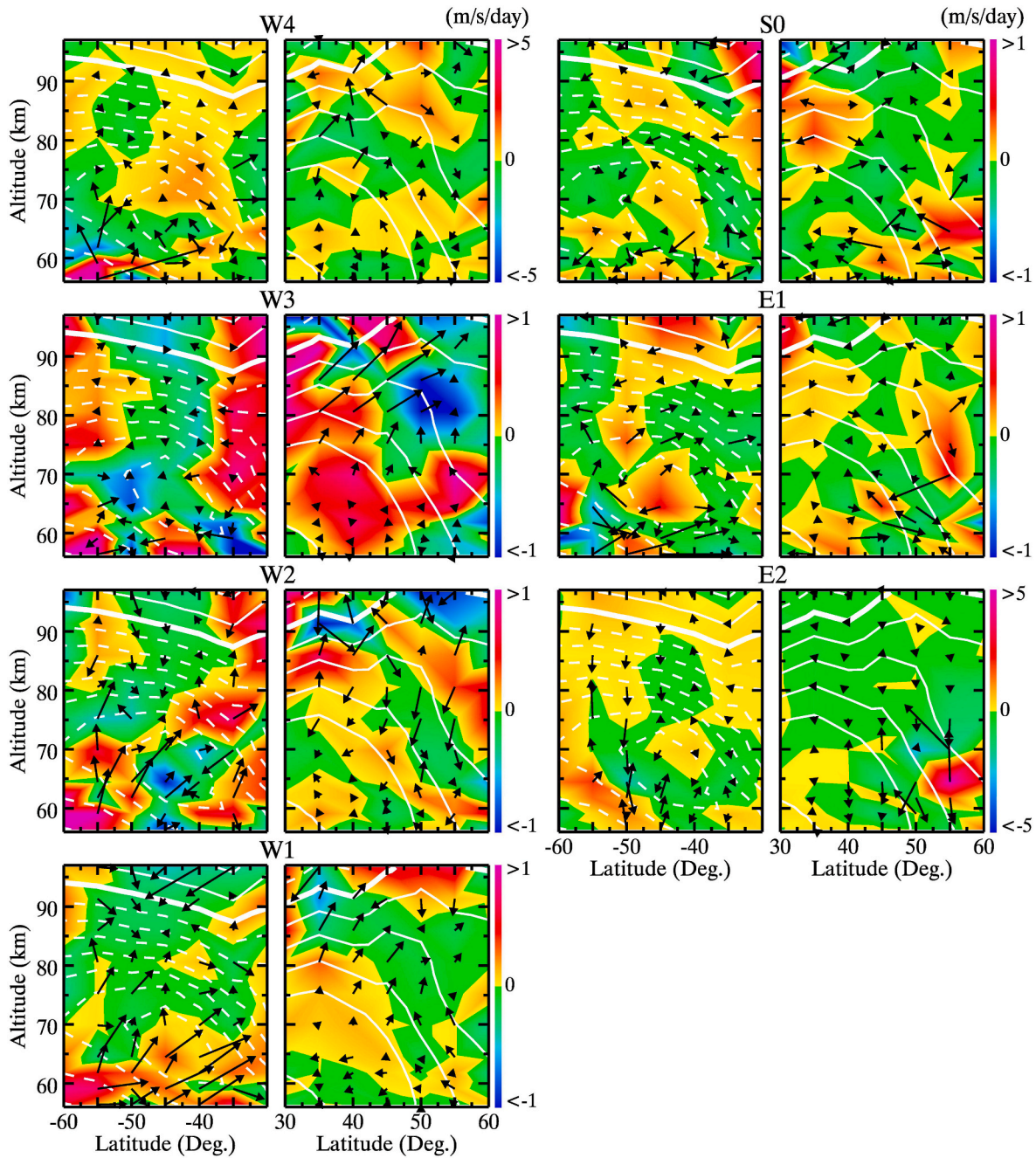


Fig. 9. Same as Fig. 10, but for 28 July.

and radar winds did not agree in either amplitude or phase. As described in Fritts et al. (2019), the difference between radar and balance winds was large when short-term variabilities in amplitude or phase (period) were large, or when multiple modes equally contributed to the Q2DW. A possible reason for the disagreements is the coarse time resolution of 12 h to compute the Q2DW from MLS geopotential height data. Additionally, uncertainties of the Q2DW from observations were also large when periods of zonal wavenumber modes varied from 48 h, i. e., close to 42 or 56 h because the Q2DWs were estimated by least-square fits to sinusoids with a period of 48 h.

4. Discussion

It has been already reported that the Q2DW is enhanced in January and July in both northern and southern hemispheres, with especially

strong responses for the meridional component in January in the southern hemisphere due to enhancements of W3. Our results showed larger amplitudes in the northern hemisphere in January than July and for the zonal component than the meridional component (Fig. 3). These enhancements were a mixture of mostly W4, W3, W2, and W1 (Figs. 4 and 5).

Gurubaran et al. (2001b) reported Q2DW responses stronger in winter than summer at Tirunelveli (9°N, 78°E). If the Q2DW is generated in summer hemisphere and propagates to winter hemisphere (Craig et al., 1983; Rao et al., 2017), Q2DW responses at Tirunelveli are larger when propagated from the summer southern hemisphere than generated in the summer northern hemisphere.

Nozawa et al. (2003a, 2003b) analyzed Q2DW employing MF radar wind measurements at Tromsø (70°N, 19°E) and Poker Flat (65°N, 148°W) from 1998 to 2002 and found stronger responses in winter.

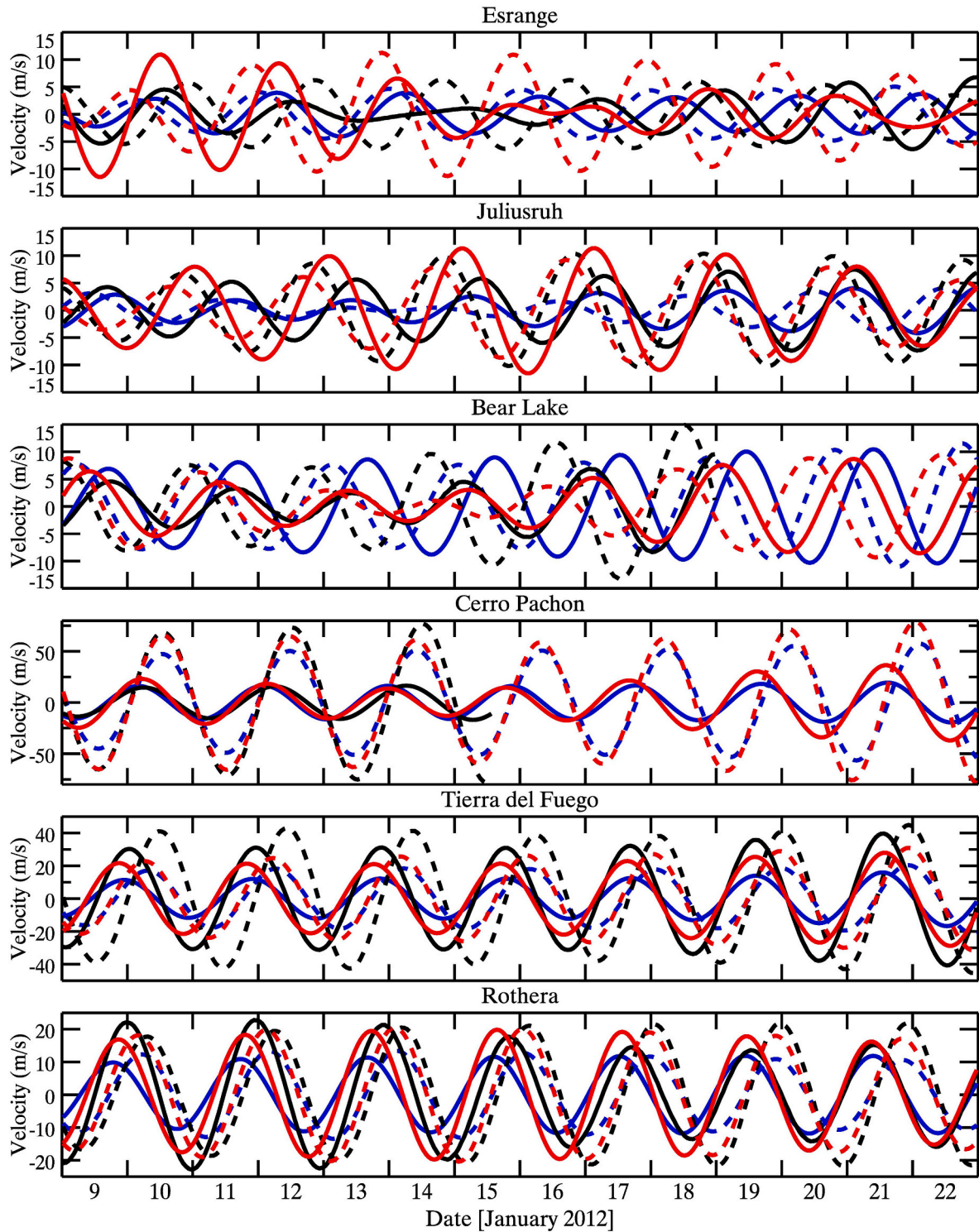


Fig. 10. Time series of Q2DW in meteor radar winds at Esrange, Juliusruh, Bear Lake, Cerro Pachón, Tierra del Fuego, and Rothera at 90 km, and balance winds at closest latitudes at 91 km from 9 to January 22, 2012. Solid and dashed lines are for zonal and meridional winds, respectively. Black, red, and blue indicate meteor radar Q2DWs, balance wind Q2DWs, and W3, respectively.

Tunbridge and Mitchell (2009) found significant interannual variability of Q2DW responses from meteor radar wind measurements at Esrange ($68^{\circ}\text{N}, 21^{\circ}\text{E}$), which is close to Tromsø, from 1999 to 2008. According to Tunbridge and Mitchell, summer amplitudes were much larger than amplitudes in January and February in 2000, 2002, 2003, 2005, and 2007, and winter amplitudes were equal to or greater than summer amplitudes in 2004 and 2006. Specifically, their observations revealed

that Q2DW responses from late November 2007 to late January 2008 were stronger than responses in July 2007 and 2008. Questions remain concerning interannual variability of Q2DW amplitudes. Nonetheless, because the Q2DW is a superposition of different zonal wavenumbers during summer in the northern hemisphere (Ern et al., 2013), it is possible that amplitudes of each zonal wavenumber may have significant seasonal and interannual variabilities. Unfortunately, based upon

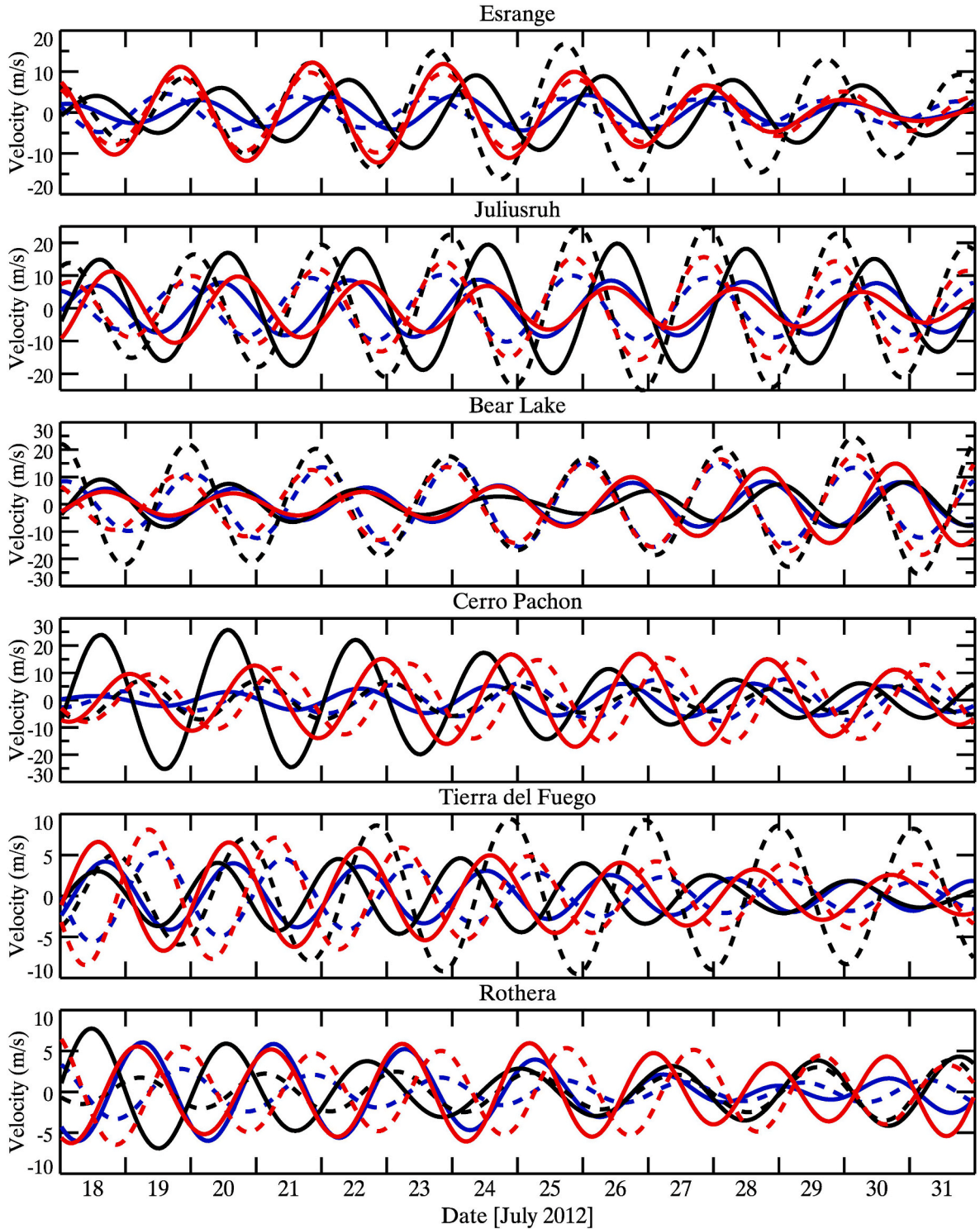


Fig. 11. Same as Fig. 10, but from 18 to July 31, 2012.

ground measurements at a single site, it is impossible to extract amplitudes of each zonal wavenumber. However, the Q2DW has a significant longitudinal variability when multiple zonal wavenumbers contribute to the Q2DW (Figs. 6 and 7). In fact, our results showed that W3 maximized in July in the northern hemisphere, while W3 amplitudes were still comparable to other zonal wavenumbers. Q2DW amplitudes in July are significantly enhanced when different zonal wavenumbers are inphase and suppressed when they are anti-phase.

Our results showed somewhat smaller amplitudes of W4 and W2 in

July in the northern hemisphere than expected from previous studies. This is likely because we used least square fits to a fixed period of 48 h even though periods of the W4 and W2 Q2DW may have been beyond our period. Fig. 4 shows amplitude enhancements for meridional W4 in early February at $<50^{\circ}$ S. This does not necessarily mean that the meridional W4 Q2DW maximized, but that the meridional W4 at a period of 48 h was maximized. Recently, Pancheva et al. (2018) found the eastward propagating zonal wavenumber 3 (E3) Q2DW at 50° and between 60 and 70 km as a winter phenomenon in a geopotential height

field employing Aura/MLS observations. According to nonlinear interaction theory, the E2 Q2TDW is generated by an interaction between the migrating (W1) diurnal tide and W3 Q2DW. Similarly, the E3 Q2DW can be generated by the interaction between the W1 diurnal tide and W4 Q2DW (Pancheva et al., 2018). If this is correct, the E3 Q2DW will not appear in our analyses from the least square fittings with the 48-h period, however we could not find influence of E3 on Q2DW wind fields in the MLT even by changing a period to 42 h.

Instead, we found the W1 and S0 Q2DW in both hemispheres. We diagnosed aliasing between the W3, and W1 and S0, and then concluded that these were not aliased. In particular, the balance wind Q2DWs differed to a greater degree from the radar wind Q2DWs without either S0 or W1. Unfortunately, we cannot infer any possible generating mechanisms for W1 and S0 at present but plan to explore this aspect in future work.

Our analyses poleward of 30° showed moderate Q2DW enhancements in September and early May in the southern hemisphere (Figs. 1 and 2), especially in the zonal component. These were a mixture of enhancements of westward propagating zonal wavenumbers. Q2DW responses at low and equatorial latitudes were analyzed employing ground-based radar data at Thumba (9°N , 77°E) from 2006 to 2009 by Babu et al. (2011), at Thumba and Kototabang (0° , 100°E) from 2006 to 2012 by Kumar et al. (2018), at Thumba from 2005 to 2014 and Tirunelveli from 1993 to 2009 by Rao et al. (2017), and at Kolhapur (17°N , 74°E) from 2013 to 2017 by Gaikwad et al. (2019). All of these researchers found amplitude enhancements in October, in addition to January and July. Particularly, Kumar et al. (2018) estimated primary zonal wavenumbers, that is, W3, W4, and W2 in January, July, and October, respectively. Lima et al. (2004) analyzed meteor radar data at Cachoeira Paulista (23°S , 45°W) from April 1992 to March 2002 and found enhancements only in summer and winter. Araújo et al. (2014), on the other hand, compared Q2DW responses at São João do Cariri (7°S , 37°W) with those at Cachoeira Paulista and found that the Q2DW was enhanced in both summer and winter at the two sites, but in March and October only at São João do Cariri. This implies that the Q2DW in boreal autumn at equatorial latitudes can propagate poleward in both hemispheres, but that the Q2DW in austral autumn propagates only to low latitudes in the southern hemisphere.

To study correlations of the Q2DW in the MLT and at the stratosphere, we analyzed Q2DW structure at lower altitudes between 30 and 60 km. Our results showed that the Q2DW was enhanced in winter with larger amplitudes in the southern hemisphere than the northern hemisphere. Maximum amplitudes of W3 were ~ 18 m/s in the zonal wind and ~ 22 m/s in the meridional wind at $\sim 40^\circ\text{S}$ and ~ 50 km in July. On the other hand, maximum amplitudes at 40°N were ~ 10 m/s for both components in January. Madhavi et al. (2015) studied structure of the stratospheric Q2DW at middle and high latitudes in both northern and southern hemispheres using Global Positioning Radio Occultation (GPSRO) Constellation Observing System for Meteorology, Ionosphere, and Climate (COSMIC) data during an interval from November 2006 to December 2010. They found enhancements in winter in both hemispheres with large interannual variability in amplitude. Limpasuvan et al. (2005) analyzed global structure of the Q2DW employing MLS data in water vapor, carbon monoxide, temperature, and line-of-sight wind from December 2004 to March 2005, and inferred that the Q2DW in winter hemisphere is mainly trapped in the stratosphere and lower mesosphere. This implies a different generation mechanism of the Q2DW between the MLT and the stratosphere.

The Q2DWs between the stratosphere and the MLT also differed in vertical structures. In January in the southern hemisphere, the meridional W3 Q2DW in the MLT exhibited upward propagation with a vertical wavelength of ~ 70 km at $<60^\circ\text{S}$ and downward propagation at $\geq 70^\circ\text{S}$. In the stratosphere, on the other hand, the W3 Q2DW was evanescent in both hemispheres.

Planetary waves are expected to be enhanced by baroclinic/barotropic instabilities. A necessary condition for the instabilities is the

meridional gradient of the quasi-geostrophic potential vorticity (q_φ) < 0 (Liu et al., 2004; Yue et al., 2012a), which is derived from an equation

$$q_\varphi = 2\Omega \cos\varphi - \{[(\bar{u} \cos\varphi)_\varphi / (a \cos\varphi)]_\varphi + a/\rho [(f^2 / N_2) \rho \bar{u}_z]_z\}, \quad (8)$$

where N is the Brunt-Väisälä frequency, and ρ is density. We obtained $q_\varphi < 0$ in January only at 40°S and < 80 km, agreeing with Gu et al. (2016) and Liu et al. (2004), and $q_\varphi > 0$ in July in the northern hemisphere. According to equation (8), the second term must be greater than the first term for $q_\varphi < 0$. However, the second term is negative, except for < 80 km at $\sim 40^\circ\text{S}$.

The second term in the meridional component of the EP flux equation (Equation (6)) was larger in magnitude than the first term at 91 km in January in the southern hemisphere, and hence the meridional component depends primarily on u' and v' amplitudes. Meridional fluxes for W3 increased with altitude and reached > 100 m 2 /s 2 in January in the southern hemisphere, but increased with altitude and reached only ~ 20 m 2 /s 2 in July in the northern hemisphere due to smaller amplitudes of the Q2DW in July in the northern hemisphere.

Vertical winds at local sites have been measured by meteor radars (Egito et al., 2016; Eswaraiah et al., 2011) and reported up to a few 10 m/s. According to Yajnavalkya and Andrew (2010), vertical winds are the sum of meridional circulation, geomagnetic activity, and residual influence by short-period waves, such as gravity waves and tides, and the vertical winds in the meridional circulation are expected to be on the order of cm/s (Portnyagin et al., 2010). Therefore, the altitude component of the EP flux equation (Equation (7)) depends primarily on latitude and altitude structures of geopotential temperature and winds. Structures of the altitude component of W3 EP fluxes were similar between January in the southern hemisphere and July in the northern hemisphere, but ~ 7 times larger in magnitude in January in the southern hemisphere than July in the northern hemisphere.

Among the limited number of EP flux studies for the Q2DW in the MLT, Fritts et al. (2019) showed EP fluxes for each zonal wavenumber in the southern hemisphere on three days in January 2015. As shown in Fig. 8, their results for most zonal wavenumbers on 22 January are very similar to ours. Magnitudes for fluxes were smaller in our results than those of Fritts et al. but this is not surprising because Q2DW amplitudes in January 2015 in the southern hemisphere were larger than climatological amplitudes. Gu et al. (2016) derived EP fluxes of the Q2DW in the northern hemisphere during boreal summer in 2007 employing the ensemble data assimilation version of the Whole Atmosphere Community Climate Model + Data Assimilation Research Testbed. Their W3 EP flux structure shows upward and poleward fluxes, agreeing with our results although quantitative differences exist which are probably due to interannual variabilities. To continue this work, we plan additional study of interannual variabilities of Q2DW structure and EP fluxes.

5. Summary

We compared climatological structure and variability of the Q2DW in MLT temperature and horizontal winds for summer and winter between the northern and southern hemispheres, employing balance equations with Aura/MLS temperature and geopotential height data at latitudes between 30 and 70° and altitudes between 70 and 97 km.

Q2DW amplitudes increased with altitude in the meridional component, maximizing in summer in both hemispheres, however, we found no clear trend with altitude in the zonal component, with maxima mostly in summer. Regarding zonal and meridional components in January in the southern hemisphere, Q2DW amplitudes were dominated by W3, as previously reported. However, our results exhibited a mixture with W4 and W2 in the meridional component and with W1, S0, and E2 for the zonal component in the northern hemisphere and in winter in the southern hemisphere. Maximum amplitudes were, however, W3, most likely because we obtained amplitudes for a period of 48 h. In addition, horizontal structure of the W3 with respect to the equator was anti-

symmetric in temperature and zonal wind, and symmetric in meridional wind, indicating a Rossby-gravity normal mode.

W3 EP fluxes were poleward and upward at >85 km in summer in both hemispheres. In January in the southern hemisphere, structures of W3, W2, and W1 fluxes were similar with smaller magnitudes for W2 and W1 than W3. In July in the southern hemisphere, on the other hand, W4, W2, and W1 were somewhat similar, upward and equatorward at <70 km. In July in the northern hemisphere, though, W4, W3, and W1 fluxes showed similar structures, upward and poleward at >85 km, despite being downward and equatorward for W2.

SkiYMet was operating in January and July 2012 at three sites in each hemisphere, and the Q2DW was compared between meteor radar wind measurements and balance wind. Results agreed in the southern hemisphere in January and at lower latitudes in the northern hemisphere in July. Disagreements were larger in phases when amplitudes were smaller, multiple zonal wavenumber modes comprised the Q2DW, or Q2DW amplitudes or periods changed significantly during a short time.

Declaration of competing interest

The authors declare that they have no known competing financial interests or personal relationships that could have appeared to influence the work reported in this paper.

Acknowledgements

Research described here was funded by NSF, AGS-1647354, and NASA grants, NNX16AD89G, cited in GEMS. We also thank the EARG personnel for their invaluable help with the operation of SAAMER. We are also very grateful for the invaluable support of Jorge L. Chau and Gunter Stober at the University of Rostock, and Fabio A. Vargas at University of Illinois. The Rothera radar is running year around with the support of the British Antarctic Survey. MLS data are available online (<https://mls.jpl.nasa.gov/index-eos-mls.php>). Meteor radar data used here are available online (<http://cedar.openmadrigal.org>).

References

Andrews, D.G., Holton, J.R., Leovy, C.B., 1987. *Middle Atmosphere Dynamics*, 1st. Academic Press, San Diego, CA.

Araújo, L.R., Lima, L.M., Batista, P.P., Clemesha, B.R., Takahashi, H., 2014. Planetary wave seasonality from meteor wind measurements at 7.4°S and 22.7°S, *Ann. Geophys.* 32 (5), 519–531. <https://doi.org/10.5194/angeo-32-519-2014>.

Azeem, S.M.I., Palo, S.E., Wu, D.L., Froidevaux, L., 2001. Observations of the 2-day wave in UARS MLS temperature and ozone measurements. *Geophys. Res. Lett.* 28 (16), 3147–3150. <https://doi.org/10.1029/2001GL013119>.

Babu, V.S., Kumar, K.K., John, S.R., Subramanyam, K.V., Ramkumar, G., 2011. Meteor radar observations of short-term variability of quasi 2 day waves and their interaction with tides and planetary waves in mesosphere-lower thermosphere region over Thumba (8.5°N, 77°E). *J. Geophys. Res.* 116, D16121. <https://doi.org/10.1029/2010JD015390>.

Baumgaertner, A.J.G., McDonald, A.J., Hibbins, R.E., Fritts, D.C., Murphy, D.J., Vincent, R.A., 2008. Short-period planetary waves in the Antarctic middle atmosphere. *J. Atmos. Sol. Terr. Phys.* 70, 1336–1350. <https://doi.org/10.1016/j.jastp.2008.04.007>.

Bristow, W.A., Yee, J.-H., Zhu, X., Greenwald, R.A., 1999. Simultaneous observations of the july 1996 2-day wave event using the super dual auroral radar network and the high resolution Doppler imager. *J. Geophys. Res.* 104 (A6) <https://doi.org/10.1029/1999JA000030>, 12,715–12,721.

Chshyolkova, T., Manson, A.H., Meek, C.E., 2005. Climatology of the quasi two-day wave over Saskatoon (52°N, 107°W): 14 Years of MF radar observations. *Adv. Space Res.* 35 (11), 2011–2016. <https://doi.org/10.1016/j.asr.2005.03.040>.

Craig, R.L., Elford, W.G., 1981. Observations of the quasi 2-day wave near 90 km altitude at Adelaide (35°S). *J. Atmos. Terr. Phys.* 43 (10), 1051–1056. [https://doi.org/10.1016/0021-9169\(81\)90019-2](https://doi.org/10.1016/0021-9169(81)90019-2).

Craig, R.L., Vincent, R.A., Fraser, G.J., Smith, M.J., 1980. The quasi 2-day wave in the Southern Hemisphere mesosphere. *Nature* 287, 319–320. <https://doi.org/10.1038/287319a0>.

Craig, R.L., Vincent, R.A., Kingsley, S.P., Muller, H.G., 1983. Simultaneous observations of the quasi 2-day wave in the northern and southern hemispheres. *J. Atmos. Terr. Phys.* 45 (8–9), 539–541. [https://doi.org/10.1016/S0021-9169\(83\)80068-3](https://doi.org/10.1016/S0021-9169(83)80068-3).

Egitto, F., Andrioli, V.F., Batista, P.P., 2016. Vertical winds and momentum fluxes due to equatorial planetary scale waves using all-sky meteor radar over Brazilian region. *J. Atmos. Sol. Terr. Phys.* 149, 108–119. <https://doi.org/10.1016/j.jastp.2016.10.005>.

Eswaraiah, S., Ratnam, M.V., Murthy, B.V.K., Rao, S.V.B., 2011. Low-latitude mesospheric vertical winds observed using VHF radar. *J. Geophys. Res.* 116, D22117. <https://doi.org/10.1029/2011JD016385>.

Ern, M., Preusse, P., Kalisch, S., Kaufmann, M., Riese, M., 2013. Role of gravity waves in the forcing of quasi two-day waves in the mesosphere: an observational study. *J. Geophys. Res.* 118 (9), 3467–3485. <https://doi.org/10.1029/2012JD018208>.

Fritts, D.C., Jimura, H., Janches, D., Lieberman, R.S., Riggan, D.M., Mitchell, N.J., Vincent, R.A., Reid, I.M., Murphy, D.J., Tsutsumi, M., Kavanagh, A.J., Batista, P.P., Hocking, W.K., 2019. Structure, variability, and mean-flow interactions of the january 2015 quasi-2-day wave at middle and high southern latitudes. *J. Geophys. Res.* 124 (12), 5981–6008. <https://doi.org/10.1029/2018JD029728>.

Fritts, D.C., Isler, J.R., Lieberman, R.S., Burrage, M.D., Marsh, D.R., Nakamura, T., Tsuda, T., Vincent, R.A., Reid, I.M., 1999. Two-day wave structure and mean flow interactions observed by radar and High Resolution Doppler Imager. *J. Geophys. Res.* 104 (D4), 3953–3969. <https://doi.org/10.1029/1998JD200024>.

Gaikwad, H.P., Sharma, A.K., Gurav, O.B., Chavan, G.A., Nade, D.P., Patil, P.T., Nikte, S. S., Naniwadekar, G.P., 2019. Seasonal, annual, and interannual variability in MLT quasi-two-day waves over the low-latitude region Kolhapur (16.8°N; 74.2°E). *Adv. Space Res.* 63 (7), 2100–2117. <https://doi.org/10.1016/j.asr.2018.12.029>.

Gu, S.-Y., Li, T., Dou, X., Wu, Q., Mlynczak, M.G., Russell, J.M., 2013. Observations of quasi-two-day wave by TIMED/SABER and TIMED/TIDI. *J. Geophys. Res.* 118 (4), 1624–1639. <https://doi.org/10.1002/jgrd.50191>.

Gu, S.-Y., Liu, H.-L., Pedatella, N.M., Dou, X., Shu, Z., 2016. The quasi-2 day wave activities during 2007 boreal summer period as revealed by Whole Atmosphere Community Climate Model. *J. Geophys. Res.* 121 (7), 7256–7268. <https://doi.org/10.1002/2016JA022867>.

Guharay, A., Batista, P.P., Clemesha, B.R., Schuch, N.J., 2013. Study of the quasi-two-day wave during summer over Santa Maria, Brasil using meteor radar observations. *J. Atmos. Sol. Terr. Phys.* 92, 83–93. <https://doi.org/10.1016/j.jastp.2012.10.005>.

Gurubaran, S., Ramkumar, T.K., Sridharan, S., Rajaram, R., 2001a. Signatures of quasi-2-day planetary waves in the equatorial electrojet: results from simultaneous observations of mesospheric winds and geomagnetic field variations at low latitudes. *J. Atmos. Sol. Terr. Phys.* 63 (9), 813–821. [https://doi.org/10.1016/6826\(00\)00193-0](https://doi.org/10.1016/6826(00)00193-0).

Gurubaran, S., Sridharan, S., Ramkumar, T.K., Rajaram, R., 2001b. The mesospheric quasi-2-day wave over Tirunelveli (8.7°N). *J. Atmos. Sol. Terr. Phys.* 63, 975–985. [https://doi.org/10.1016/S1364-6826\(01\)00016-5](https://doi.org/10.1016/S1364-6826(01)00016-5).

Hagan, M.E., Forbes, J.M., Vial, F., 1993. Numerical investigation of the propagation of the quasi-two-day wave in the lower thermosphere. *J. Geophys. Res.* 98 (D12) <https://doi.org/10.1029/93JD02779>, 23,193–205.

Harris, T.J., 1994. A long-term study of the quasi-two-day wave in the middle atmosphere. *J. Atmos. Terr. Phys.* 56 (5), 569–579. [https://doi.org/10.1016/0021-9169\(94\)90098-1](https://doi.org/10.1016/0021-9169(94)90098-1).

Harris, T.J., Vincent, R.A., 1993. The quasi-two-day wave observed in the equatorial middle atmosphere. *J. Geophys. Res.* 98 (D6) <https://doi.org/10.1029/93JD00380>, 10,481–10,490.

Hecht, J.H., Walterscheid, R.L., Gelinas, L.J., Vincent, R.A., Reid, I.M., Woithe, J.M., 2010. Observations of the phase-locked 2 day wave over Australian sector using medium-frequency radar and airglow data. *J. Geophys. Res.* 115, D16115. <https://doi.org/10.1029/2009JD013772>.

Hitchman, M.H., Leovy, C.B., 1986. Evolution of the Zonal Mean State in the Equatorial Middle Atmosphere during October 1978–May 1979. *J. Atmos. Sci.* 43 (24), 3159–3176. [https://doi.org/10.1175/1520-0469\(1986\)043<3159:EOTZMS>2.0.CO;2](https://doi.org/10.1175/1520-0469(1986)043<3159:EOTZMS>2.0.CO;2).

Hitchman, M.H., Leovy, C.B., Gille, J.C., Bailey, P.L., 1987. Quasi-Stationary Zonally Asymmetric Circulations in the Equatorial Lower Mesosphere. *J. Atmos. Sci.* 44 (16), 2219–2236.

Huang, Y.Y., Zhang, S.D., Yi, F., Huang, C.M., Huang, K.M., Gan, Q., Gong, Y., 2013. Global climatological variability of quasi-two-day waves revealed by TIMED/SABER observations. *Ann. Geophys.* 31 <https://doi.org/10.5194/angeo-31-1061-2013>, 2061–1075.

Hunt, B.G., 1981. The 2-day wave in the middle atmosphere as simulated in a general circulation model extending from the surface to 100 km. *J. Atmos. Terr. Phys.* 43 (11), 1143–1154. [https://doi.org/10.1016/0021-9169\(81\)90030-1](https://doi.org/10.1016/0021-9169(81)90030-1).

Jimura, H., Fritts, D.C., Janches, D., Singer, W., Mitchell, N.J., 2015. Interhemispheric structure and variability of the 5-day planetary wave from meteor radar wind measurements. *Annales Geophysicae* 33 (11), 1349–1359. <https://doi.org/10.5194/angeo-33-1349-2015>.

Jacobi, Ch., Schminder, R., Kürschner, D., 1997. The quasi 2-day wave as seen from D1 LF wind measurements over Central Europe (52°N, 15°E) at Collm. *J. Atmos. Sol. Terr. Phys.* 59 (11), 1277–1286. [https://doi.org/10.1016/S1364-6826\(96\)00170-8](https://doi.org/10.1016/S1364-6826(96)00170-8).

Jacobi, Ch., Schminder, R., Kürschner, D., 1998. Non-linear interaction of the quasi 2-day wave and long-term oscillations in the summer midlatitude mesopause region as seen from LF D1 wind measurements over Central Europe (Collm, 52°N, 15°E). *J. Atmos. Sol. Terr. Phys.* 60 (12), 1175–1191. [https://doi.org/10.1016/S1364-6826\(98\)00076-5](https://doi.org/10.1016/S1364-6826(98)00076-5).

Jia, Y., Liu, H.-L., Change, L.C., 2012. Numerical investigation of the quasi 2 day wave in the mesosphere and lower thermosphere. *J. Geophys. Res. Atmos.* 117, D05111. <https://doi.org/10.1029/2011JD016574>.

Kulikov, M.Y., 2007. Theoretical investigation of the influence of a quasi-2-day wave on nonlinear photochemical oscillations in the mesopause region. *J. Geophys. Res.* 112, D02305. <https://doi.org/10.1029/2005JD006845>.

Kumar, K.K., Subrahmanyam, K.V., Mathew, S.S., Koushik, N., Ramkumar, G., 2018. Simultaneous observations of the quasi 2-day wave climatology over the low and

equatorial latitudes in the mesosphere lower thermosphere. *Clim. Dynam.* 51, 221–233. <https://doi.org/10.1007/s00382-01703916.2>.

Li, T., She, C.-Y., Palo, S.E., Wu, Q., Liu, H.-L., Salby, M.L., 2008. Coordinated lidar and TIMED observations of the quasi-two-day wave during August 2002–2004 and possible quasi-biennial oscillation influence. *Adv. Space Res.* 41 (9), 1463–1471. <https://doi.org/10.1016/j.asr.2007.03.052>.

Lieberman, R.S., 1999. Eliassen-palm fluxes of the 2-day wave. *J. Atmos. Sci.* 56 (16), 2846–2861. [https://doi.org/10.1175/1520-0469\(1999\)-56-2846:EPFOTD>2.0.CO;2](https://doi.org/10.1175/1520-0469(1999)-56-2846:EPFOTD>2.0.CO;2).

Lima, L., Alves, M.E.O., Batista, P.P., Clemesha, B.R., Medeiros, A.F., Buriti, R.A., 2012. Sudden stratospheric warming effects on the mesospheric tides and 2-day wave dynamics at 7°S. *J. Atmos. Sol. Terr. Phys.* 78–79, 99–107. <https://doi.org/10.1019/jastp.2011.02.013>.

Lima, L.M., Batista, P.P., Takahashi, H., Clemesha, B.R., 2004. Quasi-two-day wave observed by meteor radar at 22.7°S. *J. Atmos. Sol. Terr. Phys.* 66 (6–9), 529–537. <https://doi.org/10.1016/j.astp.2004.01.007>.

Limpasuvan, V., Dong, W.L., 2009. Anomalous two-day wave behavior during the 2006 austral summer. *Geophys. Res. Lett.* 36 (4), L04807. <https://doi.org/10.1029/2008GL036387>.

Limpasuvan, V., Wu, D.L., Schwartz, M.J., Waters, J.W., Wu, Q., Killeen, T.L., 2005. The two-day wave in EOS MLS temperature and wind measurements during 2004–2005 winter. *Geophys. Res. Lett.* 32 (17), L17809. <https://doi.org/10.1029/2005GL023396>.

Limpasuvan, V., Wu, D.L., 2009. Anomalous two-day wave behavior during the 2006 austral summer. *Geophys. Res. Lett.* 36 (4), L04807. <https://doi.org/10.1029/2008GL036387>.

Limpasuvan, V., Wu, D.L., 2003. Two-day wave Observations of UARS Microwave Limb Sounder mesospheric water vapor and temperature. *J. Geophys. Res.* 108 (D19), 4307. <https://doi.org/10.1029/2002JD002903>. *ACL* 4–1.

Li, H.-L., Talaat, E.R., Roble, R.G., Lieberman, R.S., Riggan, D.M., Yee, J.-H., 2004. The 6.5-day wave and its seasonal variability in the middle and upper atmosphere. *J. Geophys. Res.* 109 (D21), D21112. <https://doi.org/10.1029/2004JD004795>.

Madhavi, G.N., Kishore, P., Rao, S.V.B., Velicogna, I., Basha, G., 2015. Two-day wave observations over the middle and high latitudes in the NH and SH using COSMIC GPSRO measurements. *Adv. Space Res.* 55 (2), 722–731. <https://doi.org/10.1016/j.asr.2014.09.032>.

Malinga, S.B., Ruohoniemi, J.M., 2007. The quasi-two-day wave studied using the northern hemisphere SuperDARN HF radars. *Ann. Geophys.* 25 (8), 1767–1778. <https://doi.org/10.5194/angeo-25-1767-2007>.

McCormack, J.P., Coy, L., Hoppel, K.W., 2009. Evolution of the quasi 2-day wave during January 2006. *J. Geophys. Res.* 114 (D20115) <https://doi.org/10.1029/2009JD012239>.

Meek, C.E., Manson, A.H., Franke, S.J., Singer, W., Hoffmann, P., Clark, R.R., Tsuda, T., Nakamura, T., Tsutsumi, M., Hagan, M., Fritts, D.C., Isler, J., Portnyagin, Yu I., 1996. Global study of northern hemisphere quasi-2-day wave events in recent summers near 90 km altitude. *J. Atmos. Terr. Phys.* 58 (13), 1401–1411. [https://doi.org/10.1016/0021-9169\(95\)00120-4](https://doi.org/10.1016/0021-9169(95)00120-4).

Merzlyakov, E., Pancheva, D., Mitchell, N., Forbes, J.M., Portnyagin, Yu I., Palo, S., Makarov, N., Muller, H.G., 2004. High- and mid-latitude quasi-2-day waves observed simultaneously by four meteor radars during summer 2000. *Ann. Geophys.* 22 (3), 773–788. <https://doi.org/10.5194/angeo-22-1917-2004>.

Merzlyakov, E.G., Jacobi, Ch., 2004. Quasi-two-day wave in an unstable summer atmosphere – some numerical results on excitation and propagation. *Ann. Geophys.* 22 (6), 1917–1929. <https://doi.org/10.5194/angeo-22-1917-2004>.

Morris, R.J., Klekociuk, A.R., Holdsworth, D.A., 2009. Low latitude 2-day planetary wave impact on austral polar mesopause temperatures: revealed by a January diminution in PMSE above Davis, Antarctica. *Geophys. Res. Lett.* 36, L11807. <https://doi.org/10.1029/2009GL037817>.

Murphy, D.J., Vincent, R.A., 1998. Mesospheric momentum fluxes over Adelaide during the 2-day wave: results and interpretation. *J. Geophys. Res.* 103 (D22) <https://doi.org/10.1029/1998JD200001>, 28,627–628,636.

Namboothiri, S.P., Kishore, P., Igarashi, K., 2002. Observations of the quasi-2-day wave in the mesosphere and lower thermosphere over Yamagawa and Wakkanai. *J. Geophys. Res.* 17 (D16), 4320. <https://doi.org/10.1029/2001JD000539>.

Nozawa, S., Imaida, S., Brekke, A., Hall, C.M., Manson, A., Meek, C., Oyama, S., Dobashi, K., Fujii, R., 2003a. The quasi 2-day wave observed in the polar mesosphere. *J. Geophys. Res.* 108 (D2), 4039. <https://doi.org/10.1029/2002JD002440>.

Nozawa, S., Iwahashi, H., Brekke, A., Hall, C.M., Meek, C., Manson, A., Oyama, S., Murayama, Y., Fujii, R., 2003b. The quasi 2-day wave observed in the polar mesosphere: comparison of the characteristics observed at Tromsø and Poker Flat. *J. Geophys. Res.* 108 (D24), 4748. <https://doi.org/10.1029/2002JD003221>.

Pancheva, D.V., Mukhtarov, P., Siskind, D.E., 2018. Climatology of the quasi-2-day waves observed in the MLS/Aura measurements (2005–2014). *J. Atmos. Sol. Terr. Phys.* 171, 210–224. <https://doi.org/10.116/j.astp.2017.05.002>.

Pancheva, D.V., Mukhtarov, P.J., Shepherd, M.G., Mitchell, N.J., Fritts, D.C., Riggan, D.M., Franke, S.J., Batista, P.P., Abdu, M.A., Batista, I.S., Clemesha, B.R., Kikuchi, T., 2006. Two-day wave coupling of the low-latitude atmosphere-ionosphere system. *J. Geophys. Res.* 111, A07313. <https://doi.org/10.1029/2005JA011562>.

Offermann, D., Hoffmann, P., Knieling, P., Koppmann, R., Oberheide, J., Riggan, D.M., Tunbridge, V.M., Steinbrecht, W., 2011. Quasi 2 day waves in the summer mesosphere: triple structure of amplitudes and long-term development. *J. Geophys. Res.* 116 (D4), D00P02. <https://doi.org/10.1029/2010JD015051>.

Pancheva, D., Mitchell, N.J., Manson, A.H., Meek, C.E., Jacobi, Ch., Portnyagin, Yu, Merzlyakov, E., Hocking, W.K., MacDougall, J., Singer, W., Igarashi, K., Clark, R.R., Riggan, D.M., Franke, S.J., Kürschner, D., Fahrutdinova, A.N., Stepanov, A.M.,

Kashcheyev, B.L., Oleynikov, A.N., Muller, H.G., 2004. Variability of the quasi-2-day wave observed in the MLT region during the PSMOS campaign of June–August 1999. *J. Atmos. Sol. Terr. Phys.* 66 (6–9) <https://doi.org/10.1016/j.jastp.2004.01.008>, 539–565.

Pedatella, N.M., Forbes, J.M., 2012. The quasi 2 day wave and spatial-temporal variability of the OH emission and ionosphere. *J. Geophys. Res.* 117, A01320. <https://doi.org/10.1029/2011JA017186>.

Pendlebury, D., 2012. A simulation of the quasi-two-day wave and its effect on variability of summertime mesopause temperatures. *J. Atmos. Sol. Terr. Phys.* 80, 138–151. <https://doi.org/10.1016/j.jastp.2012.01.006>.

Pfister, L., 1985. Baroclinic instability of easterly jets with applications to the summer mesosphere. *J. Atmos. Sci.* 42 (4), 313–330. [https://doi.org/10.1175/1520-0469\(1985\)042<0313:BIOTW>2.0.CO;2](https://doi.org/10.1175/1520-0469(1985)042<0313:BIOTW>2.0.CO;2).

Plumb, R.A., 1983. Baroclinic instability of the summer mesosphere: a mechanism for the quasi-two-day wave? *J. Atmos. Sci.* 40 (1), 262–270. [https://doi.org/10.1175/1520-0469\(1983\)040<0262:BIOTSM>2.0.CO;2](https://doi.org/10.1175/1520-0469(1983)040<0262:BIOTSM>2.0.CO;2).

Poole, L.M.G., 1990. The characteristics of the mesospheric two-day wave as observed at Grahamstown (33.3°S, 26.5°E). *J. Atmos. Terr. Phys.* 52 (4), 259–268. [https://doi.org/10.1016/0021-9169\(90\)90093-3](https://doi.org/10.1016/0021-9169(90)90093-3).

Poole, L.M.G., Harris, T.J., 1995. The propagation of the mesospheric two-day wave in the southern hemisphere. *J. Atmos. Terr. Phys.* 57 (13), 1661–1666. [https://doi.org/10.1016/0021-9169\(95\)98845-3](https://doi.org/10.1016/0021-9169(95)98845-3).

Portnyagin, Yu I., Solov'eva, T.V., Merzlyakov, E.G., Pogorel'stev, A.I., Savenkova, E.N., 2010. Height-latitude structure of the vertical wind in the upper mesosphere and lower thermosphere (70–110 km). *Izvestiya, atmos. Ocean. Phys.* 46 (1), 85–94. <https://doi.org/10.1134/S001438311010117>.

Rao, N.V., Ratnam, M.V., Vedavathi, C., Tsuda, T., Murthy, B.V.K., Sathishkumar, S., Gurubaran, S., Kumar, K.K., Subrahmanyam, K.V., Rao, S.V.B., 2017. Seasonal, inter-annual and solar cycle variability of the quasi two day wave in the low-latitude mesosphere and lower thermosphere. *J. Atmos. Sol. Terr. Phys.* 152, 20–29. <https://doi.org/10.1016/j.jastp.2016.11.005>.

Riggan, D.A., Lieberman, R.S., Vincent, R.A., Manson, A.H., Meek, C.E., Nakamura, T., Tsuda, T., Portnyagin, Yu I., 2004. The 2-day wave during the boreal summer of 1994. *J. Geophys. Res.* 109, D08110. <https://doi.org/10.1029/2003JD004493>.

Rodgers, C.D., Prata, A.J., 1981. The quasi 2 day wave and spatial-temporal variability of the OH emission and ionosphere. *J. Geophys. Res.* 117, A01320. <https://doi.org/10.1029/2011JA017186>.

Rojas, M., Norton, W., 2007. Amplification of the 2-day wave from mutual interaction of global Rossby-gravity and local modes in the summer mesosphere. *J. Geophys. Res.* 112, D12114. <https://doi.org/10.1029/2006JD008084>.

Salby, M.L., 1980. The influence of realistic dissipation on planetary normal structures. *J. Atmos. Sci.* 37 (10), 2186–2199. [https://doi.org/10.1175/1520-0469\(1980\)037<2186:TIORD>2.0.CO;2](https://doi.org/10.1175/1520-0469(1980)037<2186:TIORD>2.0.CO;2).

Salby, M.L., 1981a. Rossby normal modes in nonuniform background configurations. *Part I. Simple fields.* *J. Atmos. Sci.* 38 (9), 1803–1804. [https://doi.org/10.1175/1520-0469\(1981\)038<1803:RNMINB>2.0.CO;2](https://doi.org/10.1175/1520-0469(1981)038<1803:RNMINB>2.0.CO;2).

Salby, M.L., 1981b. Rossby normal modes in nonuniform background configurations. *Part II. Equinox and solstice conditions.* *J. Atmos. Sci.* 38 (9), 1827–1840. [https://doi.org/10.1175/1520-0469\(1981\)038<1827:RNMINB>2.0.CO;2](https://doi.org/10.1175/1520-0469(1981)038<1827:RNMINB>2.0.CO;2).

Salby, M.L., 1981c. The 2-day wave in the middle atmosphere: observations and theory. *J. Geophys. Res.* 86 (C10), 9654–9660. <https://doi.org/10.1029/JC086iC10p09654>.

Salby, M.L., Callaghan, P.F., 2003. Dynamics of the 2-day wave in a nonlinear model of the middle and upper atmosphere. *J. Geophys. Res.* 108 (D23), 4713. <https://doi.org/10.1029/2003JD003648>.

Salby, M.L., Callaghan, P.F., 2001. Seasonal amplification of the 2-day wave: relationship between normal mode and instability. *J. Atmos. Sci.* 58 (14), 1858–1869. [https://doi.org/10.1175/1520-0469\(2001\)058<1858:SAOTDW>2.0.CO;2](https://doi.org/10.1175/1520-0469(2001)058<1858:SAOTDW>2.0.CO;2).

Sandford, D.J., Schwartz, M.J., Mitchell, N.J., 2008. The wintertime two-day wave in the polar stratosphere, mesosphere and lower thermosphere. *Atmos. Chem. Phys.* 8 (3), 749–755. <https://doi.org/10.5194/acp-8-749-2008>.

Schwartz, M.J., Lambert, A., Manney, G.L., Read, W.G., Livesey, N.J., Froidevaux, L., Ao, C.D., Bernath, P.F., Boone, C.D., Cofield, R.E., Daffer, W.H., Drouin, B.J., Fetzer, E.J., Fuller, R.A., Jarmot, R.F., Jiang, J.H., Jiang, Y.B., Knosp, B.W., Krüger, K., Li, J.-L.F., 2008. Validation of the Aura microwave Limb sounder temperature and geopotential height measurements. *J. Geophys. Res. Atmos.* 113 (D15), D15S11. <https://doi.org/10.1029/2007JD008783>.

Schröder, H., Schmitz, G., 2004. A generation mechanism for the 2-day wave near the stratosopause: mixed barotropic inertial instability. *J. Geophys. Res.* 109, D24116. <https://doi.org/10.1029/2004JD005177>.

Sonnemann, G.R., Grygalashvily, M., 2005. On the two-day oscillations and the day-to-day variability in global 3-D-modeling of the chemical system of the upper mesosphere/mesopause region. *Nonlinear Process Geophys.* 12 (5), 691–705. <https://doi.org/10.5194/npg-12-691-2005>.

Takahashi, H., Lima, L.M., Wrasse, C.M., Batista, I.S., Onohara, A., Aquino, M.G.S., Batista, P.P., Abdu, M.A., 2012. Ionospheric response to 2-day planetary wave in the equatorial and low latitude regions. *J. Atmos. Sol. Terr. Phys.* 90, 164–171. <https://doi.org/10.1016/j.jastp.2012.04.006>.

Thayaparan, T., Hocking, W.K., MacDougall, J., 1997a. Amplitude, phase, and period variations of the quasi 2-day wave in the mesosphere and lower thermosphere over London, Canada (43°N, 81°W), during 1993 and 1994. *J. Geophys. Res.* 102 (D8), 9461–9478. <https://doi.org/10.1029/96JD03869>.

Thayaparan, T., Hocking, W.K., MacDougall, J., Manson, A.H., Meek, C.E., 1997b. Simultaneous observations of the 2-day wave at London (43°N, 81°W) and Saskatoon (52°N, 107°W) near 91 km altitude during the two years of 1993 and 1994. *Ann. Geophys.* 15 (10), 1324–1339. <https://doi.org/10.1007/s00585-997-1324-3>.

Tsuda, T., Kato, S., Vincent, R.A., 1988. Long-period wind oscillations observed by the Kyoto meteor radar and comparison of the quasi-2-day wave with Adelaide HF radar observations. *J. Atmos. Terr. Phys.* 50 (3), 225–230. [https://doi.org/10.1016/0021-9169\(88\)90071-2](https://doi.org/10.1016/0021-9169(88)90071-2).

Tunbridge, V.M., Mitchell, N.J., 2009. The two-day wave in the Antarctic and Arctic mesosphere and lower thermosphere. *Atmos. Chem. Phys.* 9 (17), 6377–6388. <https://doi.org/10.5194/acp-9-6377-2009>.

Tunbridge, V.M., Sandford, D.J., Mitchell, N.J., 2011. Zonal wavenumber of the summertime 2 day planetary wave observed in the mesosphere by EOS Aura Microwave Limb Sounder. *J. Geophys. Res.* 116, D11103. <https://doi.org/10.1029/2010JD014567>.

Ward, W.E., Wang, D.Y., Solheim, B.H., Shepherd, G.G., 1996. Observations of the two-day wave in WINDII data during January, 1993. *Geophys. Res. Lett.* 23 (21), 2923–2936. <https://doi.org/10.1029/96GL02897>.

Wu, D.L., Fishben, E.F., Read, W.G., Waters, J.W., 1996. Excitation and evolution of the quasi-2-day wave observed in UARS/MLS temperature measurements. *J. Atmos. Sci.* 53 (5), 728–738. [https://doi.org/10.1175/1520-0469\(1996\)053<0728:EABOTQ>2.0.CO;2](https://doi.org/10.1175/1520-0469(1996)053<0728:EABOTQ>2.0.CO;2).

Wu, D.L., Hays, P.B., Skinner, W.R., Marshall, A.R., Burrage, M.D., Lieberman, R.S., Orlandt, D.A., 1993. Observations of the quasi 2-day wave from the high resolution Doppler imager on UARS. *Geophys. Res. Lett.* 20 (24), 2853–2856. <https://doi.org/10.1029/93GL03008>.

Yajnavalkoya, B., Gerrard, A.J., 2010. Wintertime mesopause region vertical winds from Resolute Bay (2010). *J. Geophys. Res.* 115, D00N07. <https://doi.org/10.1029/2010JD014113>.

Yue, J., Liu, H.-L., Chang, L.C., 2012a. Numerical investigation of the quasi 2 day wave in the mesosphere and lower thermosphere. *J. Geophys. Res.* 117, D05111. <https://doi.org/10.1029/2011JD016574>.

Yue, J., Wang, W., Richmond, A.D., Liu, H.-L., 2012b. Quasi-two-day wave coupling of the mesosphere and lower thermosphere-ionosphere in the TIME-GCM: two-day oscillations in the ionosphere. *J. Geophys. Res.* 117, A07305. <https://doi.org/10.1029/2012JA017815>.